
Pro gradu -tutkielma
Master's degree programme in Atmosphere-Biosphere Studies (ABS)

# A Model Study of the Global Emissions of Terpenoid Volatile Organic Compounds from Terrestrial Vegetation in the Last Millennium

Juan Camilo Acosta
Student Number: 014037027
February 2013

| | |
|---|---|
| Ohjaajat: | Prof. Ilona Riipinen |
| Tarkastajat: | Prof. Markku Kulmala |
| | Prof. Veli-Matti Kerminen |

HELSINGIN YLIOPISTO
FYSIIKAN LAITOS

PL 64 (Gustaf Hllstrmin katu 2)
00014 Helsingin yliopisto

HELSINGIN YLIOPISTO — HELSINGFORS UNIVERSITET — UNIVERSITY OF HELSINKI

| Tiedekunta/Osasto — Fakultet/Sektion — Faculty | Laitos — Institution — Department |
|---|---|
| Faculty of Natural Sciences | Department of Physics |

Tekij — Frfattare — Author
Juan Camilo Acosta

Tyn nimi — Arbetets titel — Title
A Model Study of the Global Emissions of Terpenoid Volatile Organic Compounds from Terrestrial Vegetation in the Last Millennium

Oppiaine — Lromne — Subject
Physics

| Tyn laji — Arbetets art — Level | Aika — Datum — Month and year | Sivumr — Sidoantal — Number of pages |
|---|---|---|
| Master of Science | February 2013 | 63 |

Tiivistelm — Referat — Abstract

This thesis is a global study of the changes in the plant emissions of the dominant Biogenic Volatile Organic Compounds (BVOC) in the last millennium resulting from changing environmental conditions, largely induced by humans. BVOC emitted by vegetation have multiple impacts on atmospheric chemistry and physics, for instance changes in BVOC emissions significantly change the concentrations of aerosol in continental regions, affect ozone formation and change the oxidizing capacity of the troposphere. These processes are relevant from a climate change and air quality perspectives. The variability of global fluxes of isoprene, monoterpenes and sesquiterpenes (terpenoid BVOC) over the last millennium is evaluated using the Model of Emissions of Gases and Aerosols from Nature (MEGAN). The model is driven with meteorology input data from an Earth System Model, $CO_2$ atmospheric concentrations estimated from ice samples and model reconstructions of the global changes of vegetation. The results show that global isoprene emissions have decreased 7.3%, monoterpene emissions have increased 9.8% and sesquiterpene emissions have increased 15.1% during the period 1950-1990 as compared to 1000-1800. The results suggest that the variation of isoprene emissions is governed by land-use changes, while monoterpenes and sesquiterpenes variations are dominated by temperature. Regional changes on the isoprene, monoterpene and sesquiterpene emission distribution are larger than global changes in many locations and could have had a significant impact on the chemistry and aerosol dynamic processes in the atmosphere in the last millennium. This thesis lays a basis for a future quantification of the effect on atmospheric chemistry cycles and the organic aerosol yield from biogenic organic precursors.

Avainsanat — Nyckelord — Keywords
BVOCs, SOA, Isoprene, Monoterpenes, Sesquiterpenes, Paleoclimate

Silytyspaikka — Frvaringsstlle — Where deposited

Muita tietoja — vriga uppgifter — Additional information

# Contents

# 1

# Introduction

The atmosphere of the Earth is a system in which many physical and chemical processes take place simultaneously and is in constant interaction with other systems such as the outer space, the hydrosphere, the biosphere, the soils, the lithosphere and the deep interior of the Earth. Many of the processes are interconnected through complex mechanisms and are linked in a variety of ways. This thesis focuses on one branch of this process, the exchange of organic compounds between atmosphere and biosphere. This process links the biological response of the terrestrial vegetation to climate and land-use changes in the last millennium.

An important group of the organic compounds exchanged by the atmosphere and biosphere are the Biogenic Volatile Organic Compounds (BVOC). By definition, BVOC are all the gaseous organic compounds emitted by living organisms excluding methane (Kesselmeier et al., 1999). The large majority of BVOC are emitted by terrestrial vegetation (Seinfeld and Pandis, 2006), these compounds enter the atmosphere in a reduced state that makes them an easy target for chemically active oxidizing compounds like the hydroxyl radical, nitrates and ozone. As a general rule, BVOC split and react in the atmosphere until they oxidize forming carbon dioxide, unless intermediate gaseous products are condensed into aerosol phase or are deposited beforehand (Peñuelas et al. 2010). The organic carbon exchange between terrestrial vegetation and the atmosphere is therefore an important driver of the physical processes and chemical reactions that take place in the lower atmosphere and can ultimately affect the evolution of the climate from local to global scales (Kulmala et al., 2004, Peñuelas et al., 2009, Peñuelas et al., 2010, Arneth et al., 2010). The figure 1.1 explained in chapter 2, depicts the main mechanisms behind BVOC emissions, their atmospheric processing, their subsequent effects on climate and its feedback on BVOC emissions.

Historically, global BVOC emissions throughout the Holocene have been estimated in few specific periods (Adams et al., 2001, Kaplan et al., 2006, Valdez et al., 2005). The studies agree on having

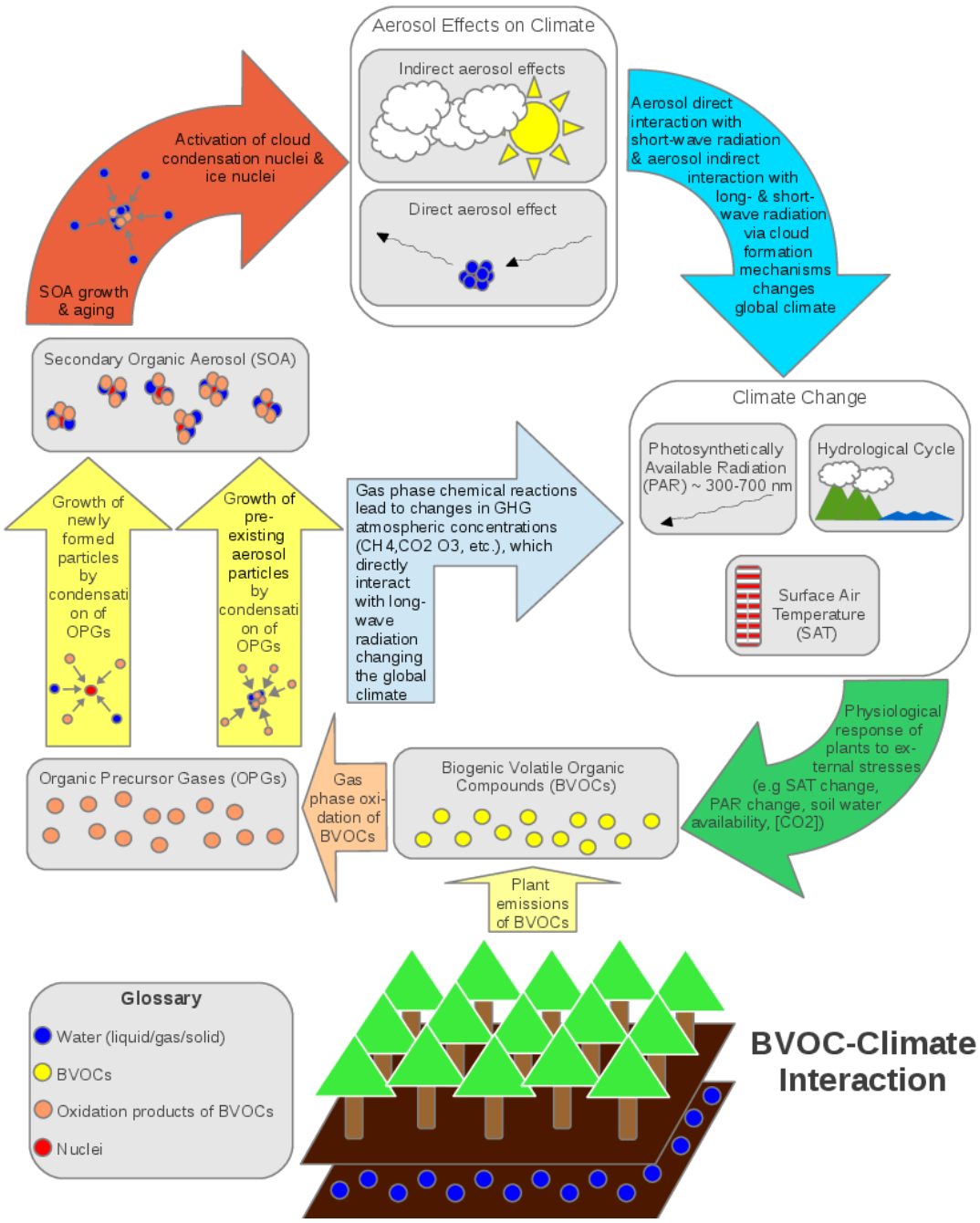


**Figure 1.1:** Terrestrial BVOC emissions-climate feedback. BVOC are emitted by vegetation (light yellow arrow), their emission activity depends on canopy temperature, incoming solar radiation, soil water availability (precipitation dependent) and $CO_2$ concentration. After being emitted, BVOC are oxidized in the atmosphere (light pink arrow) and converted into low-volatile and semi-volatile compounds which condense into aerosol phase (yellow arrow). Aerosols affect the climate directly and indirectly by changing cloud properties (red, blue arrows). GHG concentrations such as methane and ozone are affected by changing emissions of BVOC trough gas-phase chemistry processes. Changing GHGs lead to climate change (light blue arrow). Climatic variables affect emissions of BVOC by plants (green arrow).

significantly lower total BVOC global emissions during the last glacial maximum (about 21000 years ago) than before the industrialization. At the last glacial maximum BVOC emission estimates ranged from 575 to 730 Tg $yr^{-1}$, before the industrialization, the emission estimates ranged from 950 to 1160 Tg $yr^{-1}$. All this due to a lower coverage of the Earth with natural potential vegetation and a lower air temperature. BVOC historical reconstructions must rely on models because no direct BVOC proxies have been found. The atmospheric lifetimes of BVOC displayed in table 1.1 impose a major limitation for BVOC to mix evenly in the atmosphere and be transported to distant regions. If any proxy is found, the uneven global concentrations of the chemical species have to be determined through measurements in many different locations.

Studies estimate hundreds or even thousands of chemical species of BVOC (Laothawornkitkul et al., 2009). They differ in size, structure and chemical properties, making their study a challenging task. Among the different BVOC families, Isoprene (IP) and Monoterpenes (MT) are the most widely studied because they are highly reactive and are important contributors to the total BVOC flux from terrestrial vegetation (Laothawornkitkul et al., 2009). Roughly, IP accounts for half of the global terrestrial BVOC emissions (467-681 Tg $yr^{-1}$), while MT emissions are less certain. According to model predictions, MT global fluxes vary between 36 and 140 Tg $yr^{-1}$ (Arneth et al., 2009). Table 1.1 shows the current estimated limits to global emissions, lifetimes and concentrations for the main BVOC families (Laothawornkitkul et al., 2009), (Kesselmeier et al., 1999), (Arneth et al., 2008).

This work is focused in the emission of terpenoid BVOC: Isoprene (IP), Monoterpenes (MT) and Sesquiterpenes (ST). IP molecule is shown in figure 1.2, it consists of a five carbon backbone with eight hydrogen atoms ($C_5H_8$). It is produced by enzymes inside the plant cells and released almost entirely after being synthesized (Fall et al., 1992). MT and ST consist of several compounds with 10 and 15 Carbon atom molecules respectively ($C_{10}$ and $C_{15}$) (Some abundant MT and ST are displayed in figure 1.2). MT and ST are also produced inside the plants cells, but unlike IP,

**Table 1.1:** Atmospheric concentrations, lifetimes and global emissions of Biogenic Volatile Organic Compounds (BVOC).

| **Compound Family** | **Chemical lifetime** Day | Night | **Global Emissions** Tg $yr^{-1}$ | **Atmospheric Concentrations** |
|---|---|---|---|---|
| Isoprene | 3 hr | 1.5 hr | 467-681 | ppt to several ppb |
| Monoterpenes | < 5-180 min | < 2-30 min | 36-140 | ppt to several ppb |
| Sesquiterpenes | < 4 min | < 2 min | N.A. | Too reactive to be measured |
| Other reactive VOC | < 1 day | N.A. | 295 | 1-3 ppb |
| Other VOC | > 1 day | N.A. | 295 | 2-30 ppb |

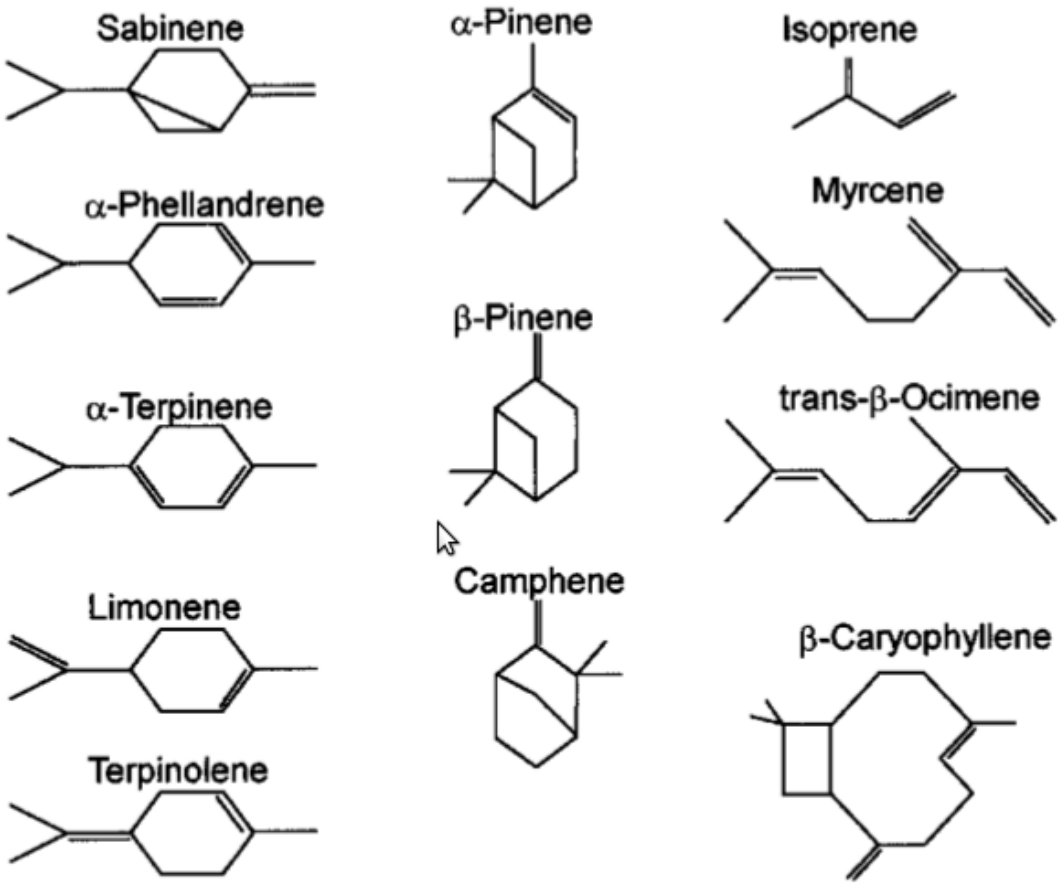


**Figure 1.2:** Molecules of the BVOC: isoprene ($C_5$), some monoterpenes ($C_{10}$) and sesquiterpene $\beta$-Caryophyllene ($C_{15}$). Figure taken from Kesselmeier et al. (1999).

MT and ST are mostly released from hydrocarbon reservoirs in resin ducts, glands or trichomes (plant outgrowths), meaning that their emission is mostly dependent on reservoir emissivity instead of the synthesis rate. Under similar climate conditions, BVOC emissions change widely over plant type. Generally, terpenoid BVOC emissions have a strong dependence on canopy air temperature (Sharkey et al. 2001). Additionally, the photosynthetically available radiation (PAR) has an enhancing effect on emissions from IP producing species. A PAR dependence of MT and ST emitting plants depends on chemical compound. For instance MT producing plant species like slash pine have a sensitive response to leaf temperature and no dependence on light, having non zero emissions during nighttime (Tingey et al., 1980). In contrast, empirical evidence suggests that for large scale modeling studies a similar overall light response of MT and ST emissions can be used with a Light Dependency correction Factor (LDF) explained in section 3.4 (Kesselmeier et al., 1999). $CO_2$ atmospheric concentrations and drought inhibit IP emissions, while MT and ST response are far from conclusive and the effects are still unknown (Peñuelas et al., 2010). Therefore, this study considers these two effects only on IP emissions.

## 1.1 Objectives of this Work

This thesis presents a time-continuous millennial reconstruction of the global emission of terpenoid BVOC, using meteorology and land cover input data from state-of-the-art numerical Earth System and Dynamic Global Vegetation models and carbon dioxide estimates to drive an empirical model that simulates the organic carbon exchange response of terrestrial vegetation to external environmental stresses. The main objective of this work is to identify and quantify the human effect on the terrestrial emissions of terpenoid BVOC species by answering the following questions:

1. How have the global emissions of terpenoid BVOC (IP, MT and ST) varied in the last millennium?
2. Which factors (climate, land-use, soil water availability and carbon dioxide concentrations) are the main drivers of this variability?
3. How has the regional distribution of terpenoid species varied?
4. What are the limitations and advantages of the estimates?

# 2

# Background and Theory

## 2.1 BVOC-Climate feedback via gas phase chemistry

The vegetation cover of the earth has been transformed throughout history by agricultural practices resulting in a change of the chemical composition of the atmosphere (Kaplan et al., 2010). Additionally, changes in surface air temperature, photosynthetic solar radiation at the surface and soil water moisture on the planet affect the biological activity of plants leading to different organic carbon emissions worldwide (Kaplan et al., 2010). BVOC play a relevant role in atmospheric chemistry by reacting with the major oxidants of the lower atmosphere: the OH radical and tropospheric ozone ($O_3$). OH and $O_3$ concentrations change with varying BVOC emissions in chemical cycles mediated by mono-nitrogen oxides ($NO_X$) present in the air (Laothawornkitkul et al. 2009). Tropospheric $O_3$ is an important greenhouse gas (GHG) and a major pollutant. Additionally, some authors point out that BVOC are more efficient sinks for OH radical than methane, meaning that at high concentrations of BVOC, methane has longer residence times in the atmosphere (Fehsenfeld et al., 1992, Adams et al., 2001, Arneth et al., 2008). Methane is also a powerful greenhouse gas with long atmospheric lifetime (8.4 years). (IPCC Report, 2007). GHG absorb and re-radiate outgoing thermal radiation from the surface of the Earth and atmosphere exerting a positive climate forcing. A positive climate forcing means that the temperature of the air increases because there is a positive imbalance on top of the atmosphere between the incoming and outgoing energy in the the form of electromagnetic radiation. A negative climate forcing has an opposite effect on temperature. The climate effect of BVOC on climate via air chemistry is represented in figure 1.1 by the central light blue arrow.

## 2.2 BVOC-Climate feedback via aerosol formation

Gas-phase reactions of BVOC with the atmosphere oxidants produce semi-volatile and low-volatile compounds that form atmospheric aerosols. Aerosols are liquid or solid particles suspended in the air, they vary in size, shape and chemical composition, their dimensions span five orders of magnitude approximately, from 1 to $10^5$ nm. This range has been divided in imaginary approximate boundaries according to their mean diameter to characterize their size distribution. Particles between 1 and 20 nm are classified as nucleation mode aerosols, between 20 and 100 nm are Aitken mode aerosols, between 100 and 1000 nm is the accumulation mode, particles larger than 1000 nm are coarse aerosols (Seinfels and Pandis, 2006). Particles in the atmosphere are also classified by their chemical composition, aerosols which contain a majority of organic carbon molecules are organic aerosol, particles with a large fraction of elemental carbon are black carbon aerosols, particles with sulfates are sulfate aerosols, particles lifted from the oceans are sea-spray and aerosols lifted from the ground are called mineral dust aerosols (Seinfels and Pandis, 2006). These definitions are sometimes ambiguous, since many aerosol particles are a mixture of different compounds and its definition is not always straightforward. Additionally, aerosols can also be classified as primary or secondary.

Particles that enter the atmosphere in a condensed phase are called primary aerosols, examples of such aerosols are: sea spray, dust, pollen, volcanic ash or soot from industries, vehicles or natural fires. Secondary aerosols are formed in the atmosphere by conversion of gases to particles, they are important when investigating the climate effects of BVOC (Represented in the left of figure 1.1). Secondary aerosols are abundant in the fine modes (nucleation and Aitken) and contribute to a large fraction of the number of aerosols in the atmosphere. Five micro-physical process explained in the following paragraphs are presented in table 2.1, these processes govern the dynamics of aerosol populations in the atmosphere.

**Table 2.1:** Micro-physical aerosol processes and their effects on number and mass concentrations.

| Aerosol Physical Process | Number Concentration | Mass Concentration |
|---|---|---|
| **Aerosol Processes** | | |
| Nucleation | Increases | Increases |
| Condensation | No Effect | Increases |
| Coagulation | Decreases | No Effect |
| Wet Deposition | Decreases | Decreases |
| Dry Deposition | Decreases | Decreases |

The aerosol dynamic processes discussed in more datil below, are displayed in the left part of figure 1.1. BVOC affect the climate via formation of Secondary Organic Aerosol (SOA) through

gas-phase oxidation reactions of BVOC leading to less volatile compounds that enhance nucleation and condense onto newly formed particles or condense onto pre-existing ones (Kulmala et al., 2004). The former process changes the total number of aerosol and aerosol mass, while the latter only changes the total amount of mass in the aerosol phase but leaves the number fixed (See table 2.1). Recent studies by Kerminen et al. (2012), Riipinen et al. (2011), Carslaw et al. (2010) and Makkonen et al. (2010) strongly suggest that organic vapors support the growth of newly formed particles by nucleation to sizes in which they significantly modify the concentration of CCN. Between 20% and 90% of the total mass of aerosols with radius below 1 micrometer is organic and a large fraction of this contribution is secondary (Jimenez et al. 2009). Additionally, terpenoid BVOC (Isoprene, Monoterpenes and Sesquiterpenes) and their oxidation products are responsible for the formation of the majority of SOA making the quantification of the emissions of these gases very important (Hallquist et al., 2009). Furthermore, global climate models still fail to capture the influence on organic aerosol loadings from natural terrestrial sources. More comprehensive inventories and mechanisms for their direct emission or formation from BVOC in preindustrial pristine conditions are needed in order to characterize the climate in the past, present and future (Andreae et al., 2004).

### 2.2.1 Nucleation

Gases are constituted by molecules that move randomly and collide with each other. Some vapor molecules collide and stick together forming clusters of a few molecules, these clusters can continue growing, shrink back to single molecules or remain stable. Macroscopic ambient conditions can lead the clusters to overcome a thermodynamic phase barrier and reach a stable condensed state withing the meta-stable state of supersaturated vapor and start growing irreversibly to larger sizes, this first phase transition process is called nucleation (Vehkamäki & Riipinen 2012). The energy barrier has a maximum at a critical cluster size, if the size is exceeded the process is energetically favorable. For nucleation to happen an ambient supersaturation of the nucleating vapors must be reached in the system (Vehkamäki & Riipinen 2012).

Nucleation of molecules from vapor to liquid or solid phase is called homogeneous nucleation. Heterogeneous nucleation is mediated by foreign substances acting as nuclei, the nucleating vapor molecules form clusters on its surface. If single component clusters are growing, nucleation is unary, if two component cluster grow, nucleation is binary and if three, ternary. In addition, charged particles (ions) can also attract molecules forming clusters, this is called ion-induced nucleation. In the atmosphere, nucleation involves sulfuric acid, water and probably inorganic bases and organic acids. Atmospheric nucleation has been systematically observed in several locations all over the world and is an important source of aerosols in many continental areas

(Kulmala et al., 2004, Kulmala et al., 2007, Kulmala & Kerminen, 2008).

### 2.2.2 Condensation

After overcoming the thermodynamic barrier, the ambient supersaturation necessary for nucleation drives a net diffusive mass flux of molecules in the surroundings of the nucleated particle to its surface making it grow. This happens because the vapor pressure on the surface is less than the ambient vapor pressure of the condensing vapors.

Low volatility organic vapors are essential for nucleated particles to sustain condensation growth in the 1-100 nm range in the lower troposphere (Left yellow arrow in figure 1.1), just as water is essential for cloud droplets formed on Cloud Condensation Nuclei (CCN) to grow inside of clouds. Condensation of semi- or low-volatile organics onto larger pre-existing particles also happens in the atmosphere (Riipinen et al., 2011) (Right yellow arrow in figure 1.1), making it a sink for nucleating vapors and lowering the ambient vapor pressure that inhibits the growth of nucleated particles. The inverse effect of condensation is evaporation and reduces the size of the particles (Vehkamäki & Riipinen 2012).

### 2.2.3 Coagulation, Dry and Wet Deposition

Aerosol particles can collide with each other and stick together forming a homogeneous particle in a process called coagulation, the collisions are induced by Brownian motion of the particles, turbulence or by a difference in velocities when particles move in a same direction. In the atmosphere, Brownian coagulation is a very effective processes when small fast particles collide with larger slow ones. As a result, coagulation counteracts with the condensation growth of nucleated particles by removing them from the air before they reach climatically relevant sizes and can acts as CCN or Ice Nuclei (IN) (Red arrow on upper part of figure 1.1) (Kerminen & Kulmala, 2002).

In addition to nucleation, condensation and coagulation, two more aerosol removal processes participate in the dynamic of aerosols populations: Dry and wet deposition. Dry deposition explains how particles impact on surfaces and are removed from the air, wet deposition explains how particles are removed by impacting and sticking to precipitating drops or ice crystals. Both, dry and wet deposition are efficient removing small fast moving particles due to thermal diffusivity and large slower ones with large area, low mobility and significant gravitational settling velocities (Seinfeld & Pandis, 2006).

### 2.2.4 Direct and Indirect Aerosol Effects

The upper part of figure 1.1) displays the direct and indirect aerosol effects on climate. Aerosols directly affect the energetic balance on top of the atmosphere by scattering solar radiation back into space or by absorbing it. They can also scatter, absorb and emit long wave thermal radiation emitted from the surface of the Earth or from the atmosphere itself (Haywood et al., 2000). The scattering or absorbing capacity of an aerosol depends on optical properties determined by the size, shape, chemical composition and structure. Typically, aerosols like mineral dust, sulfate aerosols and organic carbon aerosols scatter shortwave radiation, while black carbon aerosols are highly absorbent. An increment of scattering aerosols in the atmosphere leads to a higher reflection of solar radiation back to space, creating a negative forcing and cooling down the atmosphere. Absorbing aerosols on dark surfaces like oceans or dark forests have a negative climate forcing, on bright surfaces like snow, deserts or bright clouds, absorbing aerosols have a positive climate forcing (IPCC Report, 2007). Several studies have estimated the direct climate forcing and are summarized in the IPCC Report (2007). Overall, estimates of the direct effect on climate after preindustrial times is similar in magnitude to the positive forcing exerted by methane (About 0.5 W $m^{-2}$), but the direct effect has a much larger uncertainty bar (+/- 0.4 W $m^{-2}$ Vs. +/- 0.1 W $m^{-2}$). In all cases, a larger concentrations of aerosols in the atmosphere affects the amount of solar radiation reaching the surface of the Earth by either scattering or absorbing it. A change in the solar radiation reaching the surface has potential implications on the biologic activity of vegetation.

The indirect aerosol effects are complex phenomena related to interactions between clouds and particles. Clouds can be classified in three categories: Warm clouds formed exclusively by liquid water droplets, mixed-phase clouds formed by coexisting supercooled water droplets and ice crystals, and ice clouds formed only by ice crystals. In warm and mixed-phase clouds, the water droplets are formed by the activation of CCN. The atmospheric circulation creates sustained updrafts of air masses, this process creates an expansion of a system constituted by a mixture of gases and aerosols. Prolonged and sustained updrafts lead to a cooling of the air mass and increase the relative humidity, in many cases the air mass reaches a supersaturation of water vapor (Relative humidity over 100%) meaning that thermodynamically, a fraction of the supersaturated water vapor prefers to be in liquid phase leading to an irreversible growth of CCNs to form larger droplets, this is a nucleation process followed by condensation growth. A CCN is a hygroscopic or water soluble aerosol particle such as sea salt, sulfate aerosol, aged organic aerosol or a mix on which water vapor condenses forming water droplets. These droplets are responsible

for giving the optical properties of warm clouds and the liquid water droplets of mixed-phase clouds. Small water droplets (With radius typically below 0.1 x $10^{-6}$ m) can either grow or shrink depending on the relative humidity of the air mass and the droplet size and composition. In warm clouds, an increment in the aerosol number concentration leads to higher formation of smaller cloud droplets if water content is fixed and increases the albedo of the cloud (Twomey, 2004). Additionally larger aerosols concentrations can lead to longer lifetime of clouds due to competition for water vapor (slower growth of precipitable drops) (Albrecht, 1989) and higher absorbing aerosol concentrations lead to higher evaporation rates (Hansen et al., 1997). The three effects identified in water containing cloud types are still unknown, but can exert a potential climate forcing and changes in precipitation (Lohmann et al., 2005).

Analogously to the growth of water droplets by the activation of CCN, ice crystals are formed on aerosol particles that serve as IN. Effective IN are typically larger than 0.1 x $10^{-6}$ m in diameter and are insoluble particles with a crystalline lattice like mineral dust aerosols. Ice nucleation processes are more complex than water nucleation and are not fully understood, the properties of organic aerosol suggest that liquid phase, soluble organic matter nuclei are not efficient IN, but no definite prove has been found. In the case of mixed-phased clouds and ice clouds, larger IN aerosol concentrations can create more ice nuclei that would increase on one hand the precipitation efficiency and on the other hand the riming efficiency decreases, leading to less precipitation (Rogers and Yau, 1989). The right-lower part of figure 1.1 displays the effects of a changing climate by altering the water cycle, the air temperature and the amount of solar radiation reaching the surface. All this changes create a feedback on plant activity and their BVOC emissions that subsequently affect the climate.

# 3

# Methods

## 3.1 Overview

The global emissions of terpenoid BVOC (IP, MT and ST) are estimated using the numerical Model of Emissions of Gases and Aerosols from Nature (MEGAN V2.04 (Guenther et al., 2006)) on a millennial scale with a three-hour resolution and a spatial resolution of 3.75° x 3.75°. The model was modified to include a carbon dioxide parametrization presented in Guenther et al (2012). The differences between the model used in this study and the latest version of MEGAN from Guenther et al. (2012) is the use of a less detailed standard emission inventory of each Plant

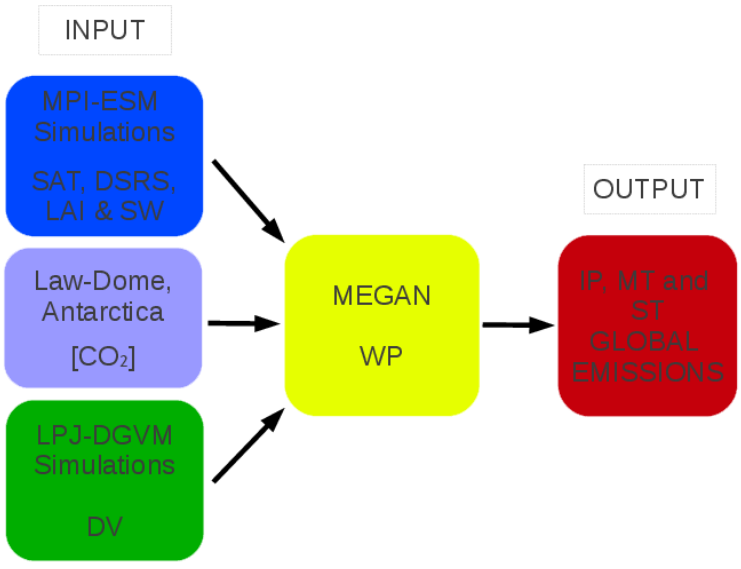


**Figure 3.1:** Model input-output schematic. Variables: Surface Air Temperature (SAT), Downward Solar Radiation at the Surface (DSRS), Leaf Area Index (LAI), Soil Water (SW) content (3m of bottom and 3m of top soil layer values averaged), Carbon dioxide concentration [$CO_2$], 11 Plant Functional Types (PFT) (8 natural + 3 anthropogenic) and Wilting Point (WP). DV = Dynamic Vegetation.

Functional Type (PFT)(section 3.3), they use 15 PFT and this study considers only 6 different PFT, and smaller monoterpene light dependency factors (section 3.4). The model is driven off-line, meaning that the input variables determine the magnitude of the total emissions for every gridbox and every time-step independently and the resulting emissions do not interact with the climate or vegetation. Figure 3.1 displays a schematic of the the model set-up. The variables Surface Air Temperature (SAT), Downward Solar Radiation at the Surface (DSRS), Soil Water (SW) (Jungclaus et al., 2010) and Leaf Area Index (LAI) (Pongratz et al., 2008, Pongratz et al., 2009) were taken from the Max-Planck Institute Earth System Model (MPI-ESM). The carbon dioxide yearly atmospheric concentrations were estimated with ice core samples from Law Dome, Antarctica (McFarling Meure et al., 2006). The vegetation maps were taken from LPJ Dynamic global Vegetation model (DV) (Kaplan et al., 2010, Pongratz et al., 2008). The soil Wilting Point (WP) fields were taken from MEGAN database (Guenther et al., 2012). The term LAI ($m^2\ m^{-2}$) refers to the ratio of projected one-sided leaf area relative to ground area and WP ($m^3\ m^{-3}$) refers to the minimum volume of water in a specific soil necessary for plants to be able to extract it. Table 3.1 describes the name, origin, temporal and spatial resolution of the input variables used in this study and table 3.2 describes the name, temporal and spatial resolution of the output variables calculated with the MEGAN algorithm. Section 3.4 gives a mathematical description of the numeric parametrization in the model.

**Table 3.1:** Input variable list with respective origin, temporal and spatial resolution. Variables: Surface Air Temperature (SAT), Downward Solar Radiation at the Surface (DSRS), Leaf Area Index (LAI), Soil Water (SW) content (3m of bottom and 3m of top soil layer values averaged), Carbon dioxide concentration [$CO_2$], 11 Plant Functional Types (PFT) (8 natural + 3 anthropogenic) and Wilting Point (WP).

| Variable Name | Units | Data Origin | Temporal Resolution | Spatial Resolution |
|---|---|---|---|---|
| SAT | °K | MPI-ESM | Daily mean values | 3.75° x 3.75° |
| DSRS | $W\ m^{-2}$ | MPI-ESM | Daily mean values | 3.75° x 3.75° |
| LAI | $m^2\ m^{-2}$ | MPI-ESM | Monthly mean values | 3.75° x 3.75° |
| SW | $m^3\ m^{-3}$ | MPI-ESM | Monthly mean values | 3.75° x 3.75° |
| $CO_2$ | ppmv | Law Dome Antarctica | Yearly mean values | 1 global value |
| 11 PFTs | % | LPJ DGVM | Yearly mean values | 0.5° x 0.5° |
| WP | $m^3\ m^{-3}$ | MEGAN | Present day values | 0.5° x 0.5° |

**Table 3.2:** Output variable list with respective temporal and spatial resolution. Variables: Isoprene emission factor (EF), monoterpenes emission factor and sesquiterpenes emission factor.

| Variable Name | Units | Temporal Resolution | Spatial Resolution |
|---|---|---|---|
| Isoprene EF | $mg\ m^{-2}\ d^{-1}$ | 3-hour values monthly averaged | 3.75° x 3.75° |
| Monoterpenes EF | $mg\ m^{-2}\ d^{-1}$ | 3-hour values monthly averaged | 3.75° x 3.75° |
| Sesquiterpenes EF | $mg\ m^{-2}\ d^{-1}$ | 3-hour values monthly averaged | 3.75° x 3.75° |

## 3.2 Climate Data

Max-Planck Institute Earth System Model (MPI-ESM) (Jungclaus et al., 2010) output climate variables shown in figure 3.1 and table 3.1 are used to drive MEGAN. MPI-ESM consists of a general circulation model for the atmosphere in which the flow of air is simulated using numerical methods in fluid dynamics. The atmospheric model is coupled with an ocean model in which exchange of energy and matter are included. MPI-ESM simulates the climate and carbon-cycle variability from year 800 to 2005 and is run on a spatial resolution of 3.75° x 3.75° grids with 19 vertical levels and a time resolution of one day. MPI-ESM captures the effects of the following known natural and anthropogenic climate forcings:

### 3.2.1 Natural Forcing

Solar forcing from the historical total solar irradiance is included in the MPI-ESM, together with an 11 year solar activity cycle due to sunspot number variation. Both physical phenomena affect the incoming radiation on top of the atmosphere. The model also contains a representation of all known periodic changes of the Earth's orbit around the sun: precession of the equinoxes, obliquity and orbital eccentricity. The nutation, a small wobble of Earth's rotational axis with a periodicity of 18.6 years is taken into account. Like solar forcing, orbital forcing modulates the incoming radiation on top of the atmosphere. Additionally, the Volcanic effect on radiation is calculated on-line in the model using satellite observations to link observed recent eruptions and optical parameter Aerosol Optical Depth (AOD). Historical AOD is estimated by the amount of sulphate in antarctic ice cores to generate time-series of volcanic activity in the past. Aerosol concentration changes due to volcanic activity scatter or absorb solar radiation influencing the radiative budget of the atmosphere.

### 3.2.2 Anthropogenic Forcing

A net climate forcing from the greenhouse gases (GHG: $CO_2, CH_4$ and $N_2O$) is considered in the model. Ozone concentrations are kept constant during the whole simulation period. The radiation effect of GHG and its climatic implications are a well constrained problem with good level of understanding among the scientific community. GHG absorb long-wave radiation emitted by the surface of the Earth and re-radiate it in all directions, this effect warms up the atmosphere.

Anthropogenic land cover changes have been estimated by the LPJ Dynamic Global Vegetation Model and are used in the MPI-ESM millennium reconstructions. Pongratz et al. (2008)

presents reconstructions of global agricultural areas and natural vegetation. Vegetation types, LAI and global distributions have an effect on Earth's surface albedo, a coefficient that measures the ratio of reflected and incoming radiation on a specific surface. Changes in vegetation cover have an effect on the reflected solar radiation by the Earth's surface altering the energy balance of the atmosphere.

The aerosol effects on the atmospheric energetic balance and its climatic implications are active fields of research. Due to the inherent complexities in aerosol physical and chemical phenomena, large uncertainty still exists. Aerosols in the model are treated in a simplified manner, only the total sulphate dry mass loading is transformed into an optical parameter to estimate the direct radiative effects. A distinction between stratospheric and tropospheric background aerosol is also made. The data between 1750 and 1850 was interpolated linearly from preindustrial times. From year 1850 to present times, loadings were based on historical reconstructions with the help of sulphate emissions. The model does not consider any interactions between clouds and aerosols neglecting all the indirect climatic effects of aerosols.

The values of MPI-ESM variables used to drive MEGAN are displayed in figure 3.2 for the Surface Air Temperature (SAT), figure 3.3 for the Downward Solar Radiation at the Surface (DSRS), figure 3.4 for the Leaf Area Index (LAI) and figure 3.5 for Soil Water (SW) mean content in the top six meters of soil. The maps on top in figures 3.2, 3.3, 3.4 and 3.5 show a millennial average of the variable and the maps below display the change between 1950-1990 and 1000-1800 averaged values. Surface Air Temperature (SAT) predictions from MPI-ESM are consistent with the 2007 IPCC report on climate change (IPCC Report, 2007), the air above the continents has warmed more than the air above the oceans and a notable Arctic amplification of the warming trend is observed in figure (3.2).

There is no obvious pattern in the Downward Solar Radiation at the Surface (DSRS) change shown in figure 3.3, a dimming of it due to scattering of the solar radiation by anthropogenic aerosols in areas where an increment of industrial activity (e.g. East Asia) has taken place between 1950 and 1990 can't be observed. Similarly, regions where air quality regulations have been implemented are expected to show an increment in the DSRS, but no clear trend is observed (Northern Europe, Eastern USA).

A large present day LAI reduction in the mid-latitudes of the northern hemisphere is predicted by LPJ DGVM and used by MPI-ESM to quantify a change in the surface albedo (Blue areas in figures 3.4). This reduction is consistent with the shrub and needleleaf tree deforestation described in the

following section. An opposite effect is observed in southeast Asia and India where present day LAI increases driven by broadleaf trees and shrub recovery (Red areas in figure 3.4). In Western USA and Australia the observed LAI increment is explained by a large change in the use of land for crops and pastures.

Changes in the amount of water available in the soil for agriculture or human use is an important aspect of climate change effects on societies all over the globe (IPCC Report, 2007). The MPI-ESM

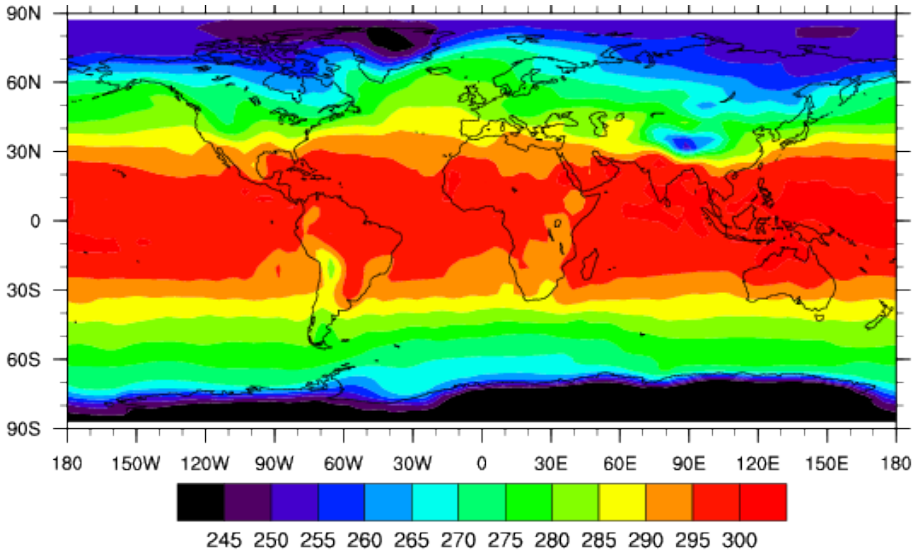


(a) Mean millennial SAT (°K)

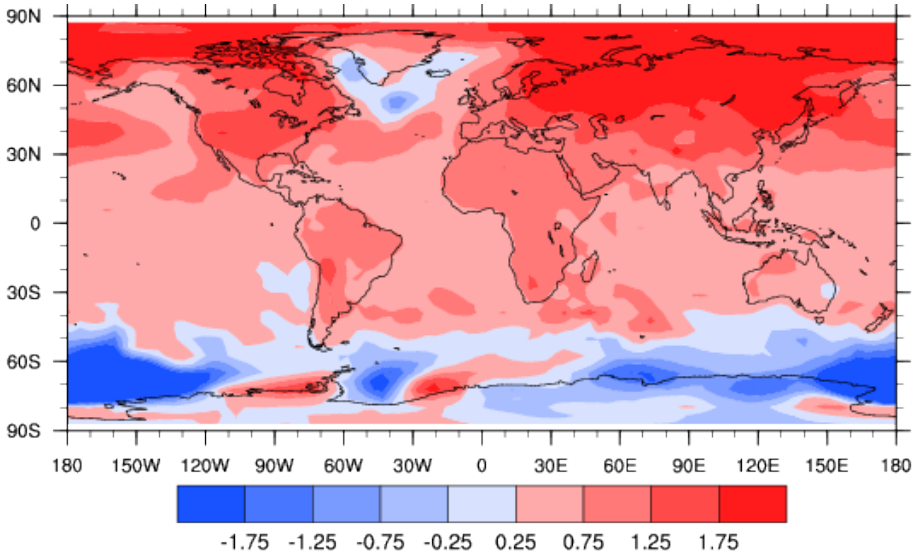


(b) Mean SAT change (°K)

**Figure 3.2:** (a) Global averaged (1000-1990) Surface Air Temperature (SAT) distribution and (b) SAT change between 1000-1800 and 1950-1990.

predicts an overall drying of arid and semi-arid regions and an increment in SW in wet and very wet regions. The averaged humidity in the top 6 m of the ground change between 1950 and 1990 as compared to preindustrial times shows a clear enhancement over wet and very wet regions and a dimming over arid and semi-arid regions associated with the rainfall variability (Figures 3.5 a and b).

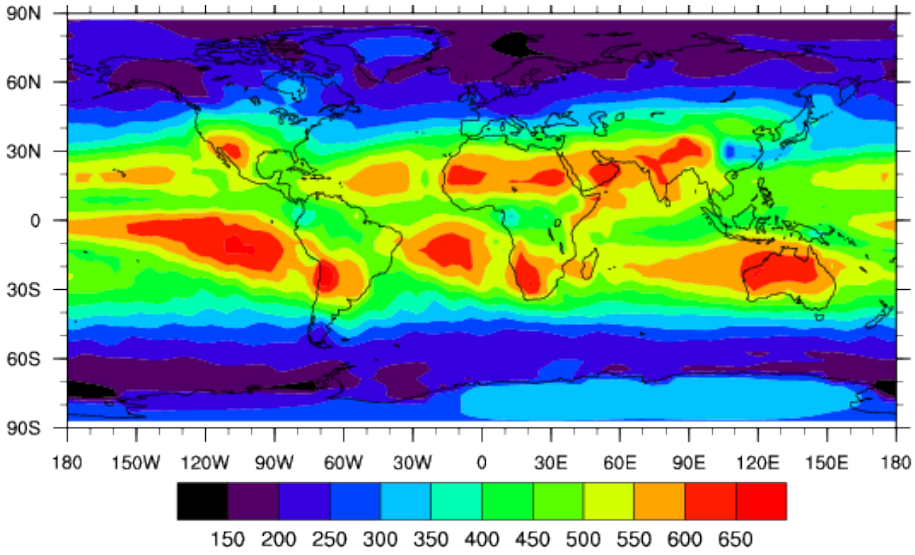


(a) Mean millennial DSRS (W m$^{-2}$)

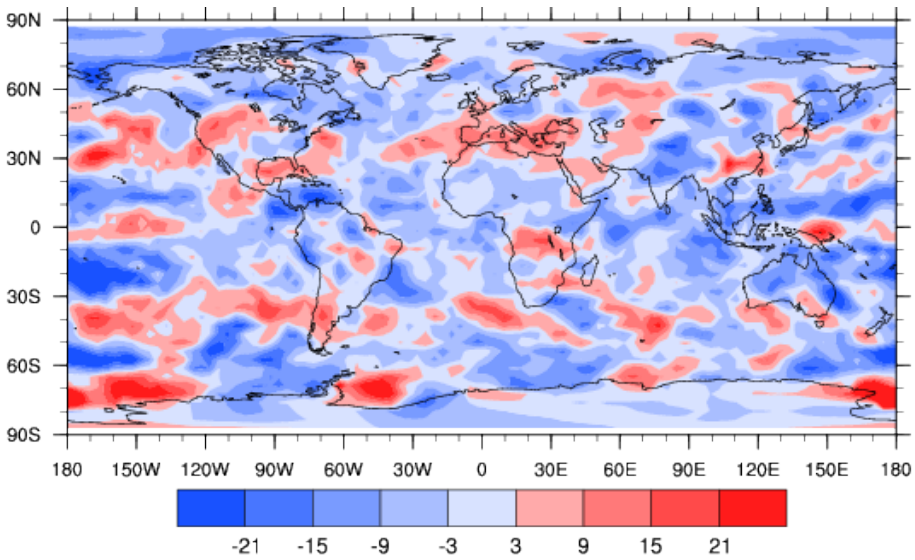


(b) Mean DSRS change (W m$^{-2}$)

**Figure 3.3:** (a) Global averaged (1000-1990) Downward Solar Radiation at the Surface (DSRS) and (b) DSRS change between 1000-1800 and 1950-1990.

## 3.3 Land-use Data

The vegetation cover of the earth has been significantly transformed throughout history by agricultural and grazing practices leading to changes in the fluxes of BVOC from terrestrial vegetation. Kaplan et al. (2010) developed an empirical method (KK10) to estimate the land-use cover of anthropogenic vegetation types (crops + pastures) using historical data on human population in the past, land suitability for agriculture based on agricultural maps and a non-linear relation between population and per capita land-use from the year 800 until the year 1850. The model estimates the

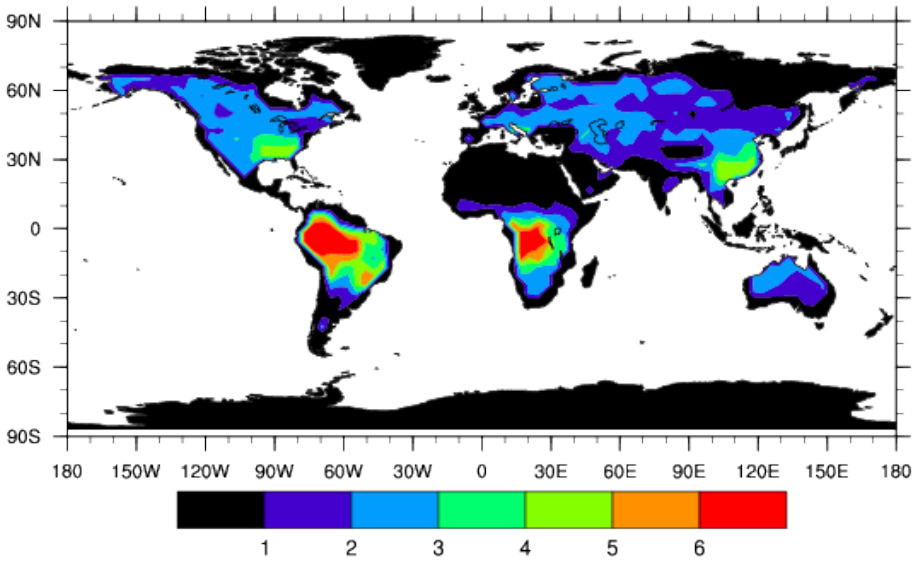


(a) Mean millennial LAI ($m^2$ $m^{-2}$)

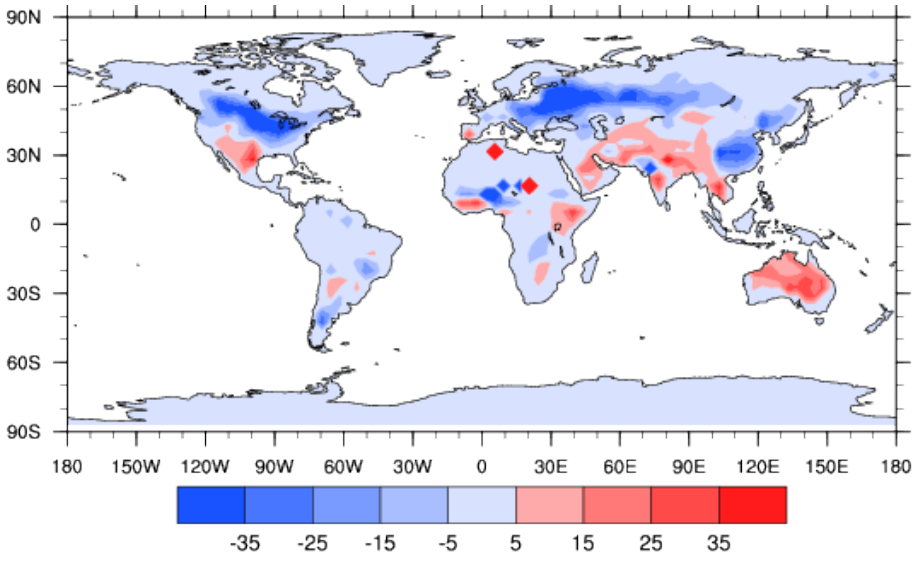


(b) Mean LAI change (%)

**Figure 3.4:** (a) Global averaged (1000-1990) Leaf Area Index (LAI) distribution and (b) LAI change between 1000-1800 and 1950-1990.

percentage of land covered by 11 vegetation types (8 natural + 3 anthropogenic), assuming that anthropogenic vegetation replaces natural potential vegetation as human populations expand or displace with time. Natural shrublands and grasses are assumed to be more suitable for animal agriculture (pasture management) due to soil properties and climate conditions, while natural forest (Broadleaf + Needleleaf tress) is assumed to be more appropriate for plant agriculture (crops). The model relies on the SAGE historical global reconstruction of the vegetation between 1850 and 2000 (Ramankutty et al., 1999, Foley et al., 2003). A full description of the model and

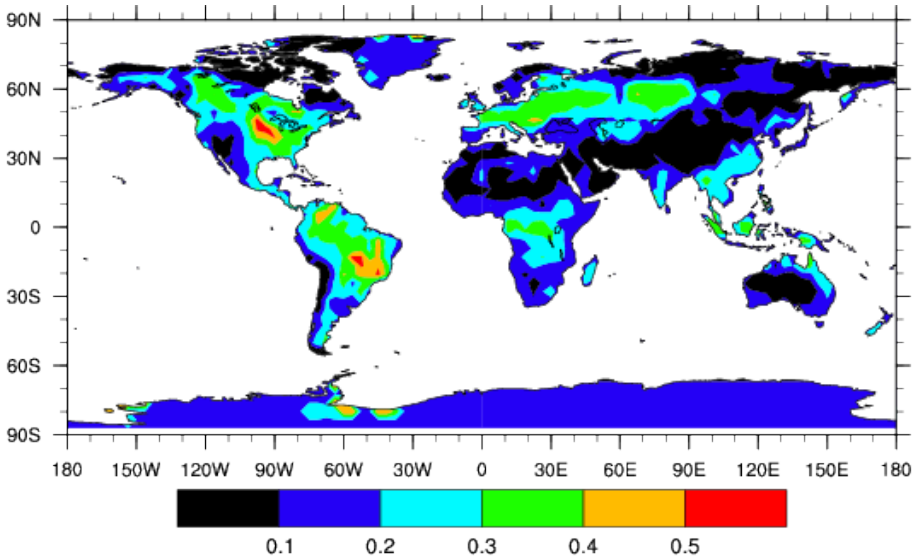


(a) Mean millennial SW ($m^3$ $m^{-3}$)

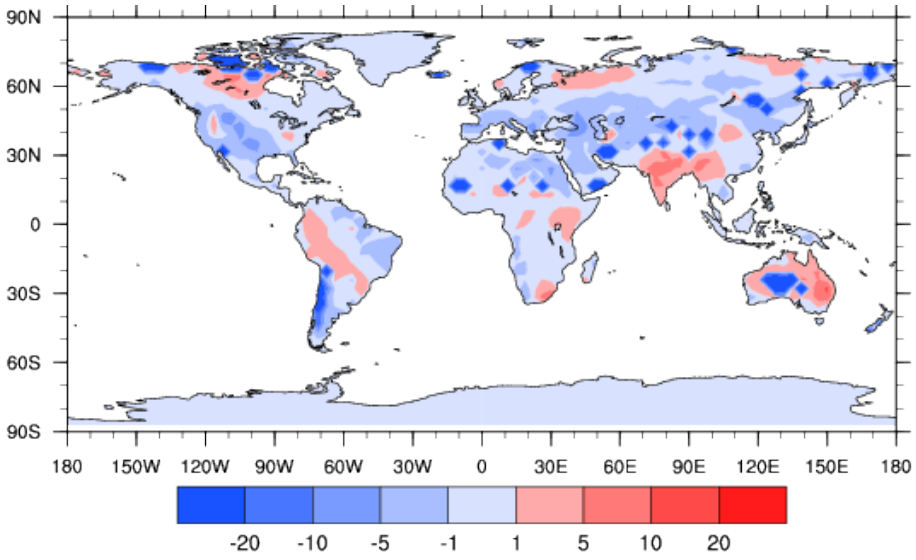


(b) Mean SW change (%)

**Figure 3.5:** (a) Global averaged (1000-1990) Soil Water (SW) content distribution and (b) SW change between 1000-1800 and 1950-1990.

methods can be found in Kaplan et al. (2010).

The vegetation maps used in this study have an annual temporal resolution, the spatial resolution was upscaled from 0.5° x 0.5° to 3.75° x 3.75°. The IP standard condition emission factors of four vegetation families were calculated following Guenther et al. (2006) and MT and ST standard emission factors of four vegetation families using Sakulyanontvittaya et al. (2008) methodology (Table 3.3). Standard conditions are explained in section 3.4. It is assumed that the emission factors stay fixed during the whole simulation period.

**Table 3.3:** Plant Functional Type (PFT) classification and IP, MT, and ST emission factors at standard conditions.

| **Plant Functional Type** | **Vegetation Type** | **IP Emission Factors** $mg\,m^{-2}\,h^{-1}$ | **MT Emission Factors** $mg\,m^{-2}\,h^{-1}$ | **ST Emission Factors** $mg\,m^{-2}\,h^{-1}$ |
|---|---|---|---|---|
| Herbaceous Plants | Pasture | 0.09 | 0.323 | 0.1 |
| Herbaceous Plants | Crops | 0.5 | 0.323 | 0.1 |
| Shrub | Natural Grass + Shrub | 10.7 | 0.735 | 0.3 |
| Needleleaf Trees | Temperate/Boreal Evergreen | 2.0 | 0.872 | 0.5 |
| Needleleaf Trees | Temperate/Boreal Deciduous | 0.7 | 0.872 | 0.5 |
| Broadleaf Trees | Tropical Evergreen | 12.6 | 0.449 | 0.3 |
| Broadleaf Trees | Tropical Deciduous | 12.6 | 0.449 | 0.3 |
| Broadleaf Trees | Temperate Evergreen | 12.6 | 0.449 | 0.3 |

The global maps in figures 3.6, 3.7, 3.8 and 3.9 show the millennial average of land covered with each PFT and its present day (1950-1990) change compared to preindustrial times. Zones all over the globe where water is scarce, are mostly covered with shrubs and small Broadleaf trees (figure 3.6 a and b). Humid high to mid-latitude land can support the growth of large boreal forests dominated by needleleaf tree species (figure 3.7 a and b), humid tropical regions have the property to support large broadleaf tree dominated rainforest (figure 3.8 a and b). Figures 3.10 and 3.11 show the temporal evolution of the 4 PFTs as classified in table 3.3 for the world and every continent respectively. The black solid line represents the total fraction of land covered with vegetation for every region, the yellow solid line represents the land fraction covered with crops and pastures (anthropogenic vegetation). The green, blue and red solid lines represent the total fraction of land covered with shrubs + natural grass, needleleaf trees, and broadleaf tress respectively (natural vegetation). Both on a regional and global scale, the land covered with anthropogenic vegetation has seen a significant increment throughout the millennium at the expense of the natural vegetation.

Figures 3.9, 3.10 and 3.11 show a consistent picture of how land management has transformed the vegetation cover of the Earth. Every continent had a larger fraction of natural vegetation and smaller anthropogenic vegetation at the beginning of the last millennium compared to the end of the millennium. The largest change in anthropogenic vegetation cover took place in Oceania where crops and pastures covered 1% of the land in the year 1000 and 58% in 1990 followed by South America changing from 10% to 35% (figure 3.11). Note that in every continent except North and Central America, the total area covered with crops and pastures represented by the yellow

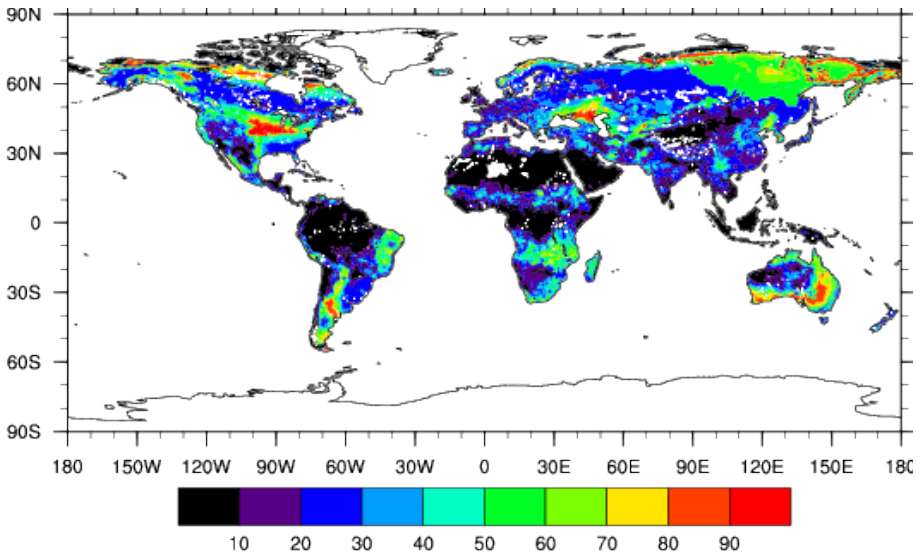


(a) Shrubs millennial cover fraction (%)

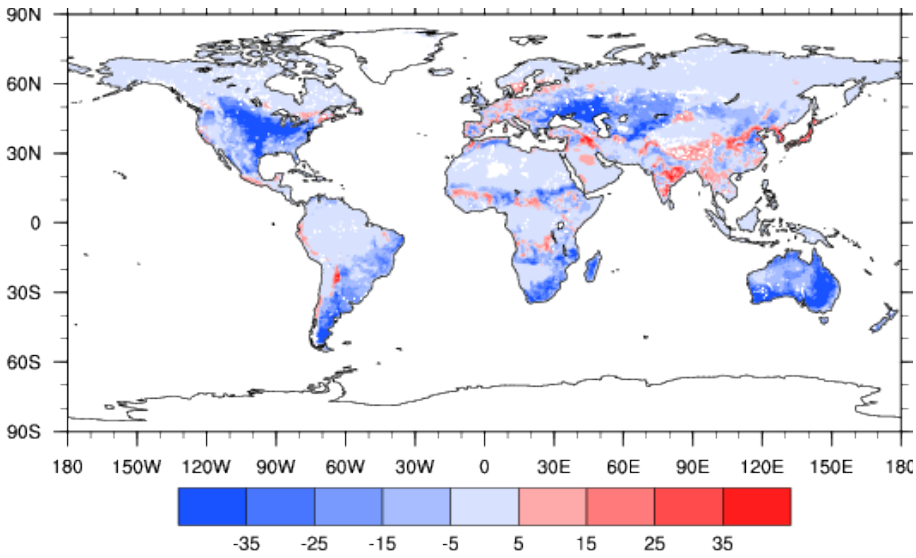


(b) Shrubs cover fraction change (%)

**Figure 3.6:** (a) Shrubs cover fraction (%) (1000-1990) and (b) Shrubs cover fraction change (%) between 1950-1990 as compared to 1000-1800.

lines in figure 3.11, have a peak just before 1850 and is manifested in the total global coverage in figure 3.10. The reason is an expected discontinuity between the modeled anthropogenic vegetation before 1850 and the estimated one from historical reconstructions taken from the SAGE database after 1850. The dynamic vegetation model over predicts in most cases the fraction of anthropogenic vegetation, however the discontinuity is small compared with the total millennial change.

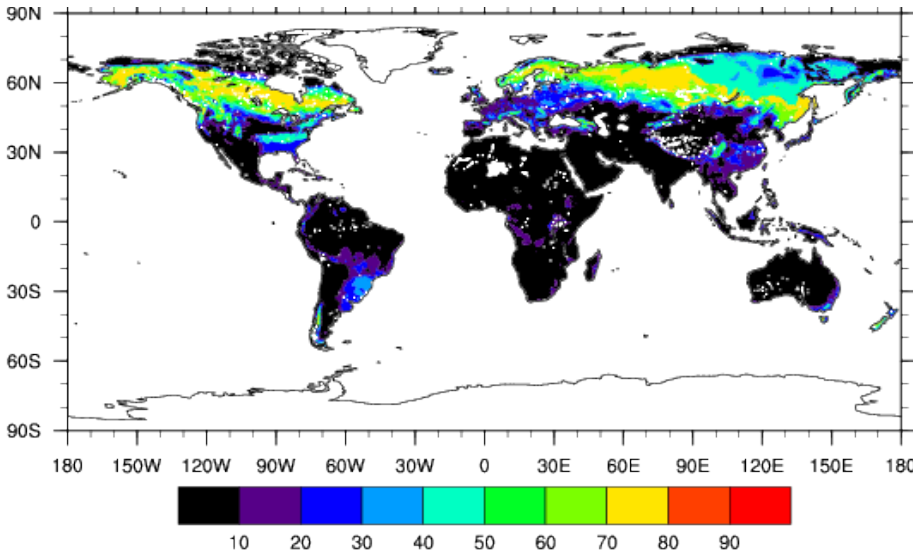


(a) Needleleaf trees millennial cover fraction (%)

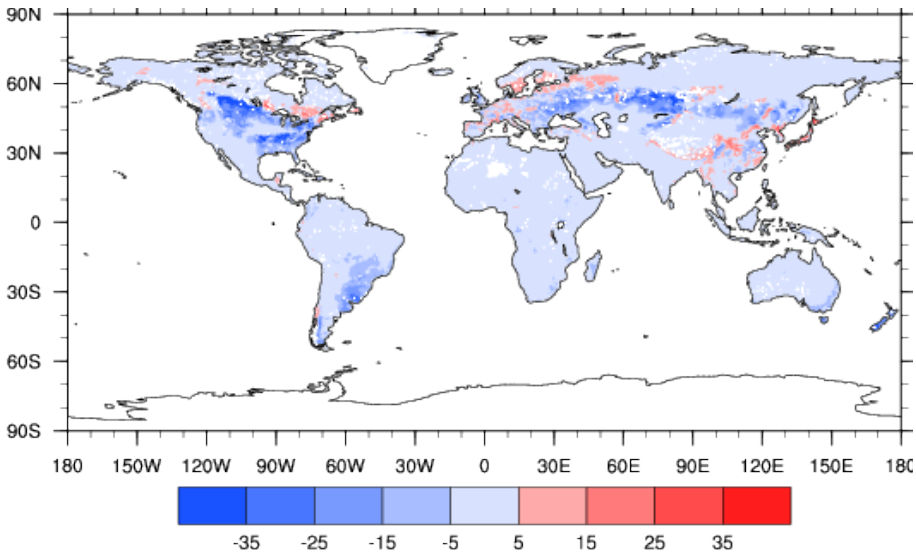


(b) Needleleaf trees cover fraction change (%)

**Figure 3.7:** (a) Needleleaf tree cover fraction (%) (1000-1990) and (b) Needleleaf tree cover fraction change (%) between 1950-1990 as compared to 1000-1800.

Every continent suffered a major land-use transformation after 1800 as a result of the population dynamics except Europe, where land-use policies of reforestation of local natural species took place (Pongratz et al., 2008). Important historical events that affected the population dynamics in continents are evident in the anthropogenic vegetation cover predicted by the model (figure 3.11). The effects of diseases on the native American population after the arrival of the Europeans to the Americas in the end of the XV century was marked by a large recovery of the natural vegetation seen in figures 3.11 a and b. Similarly, Europe suffered the black death in the XIV

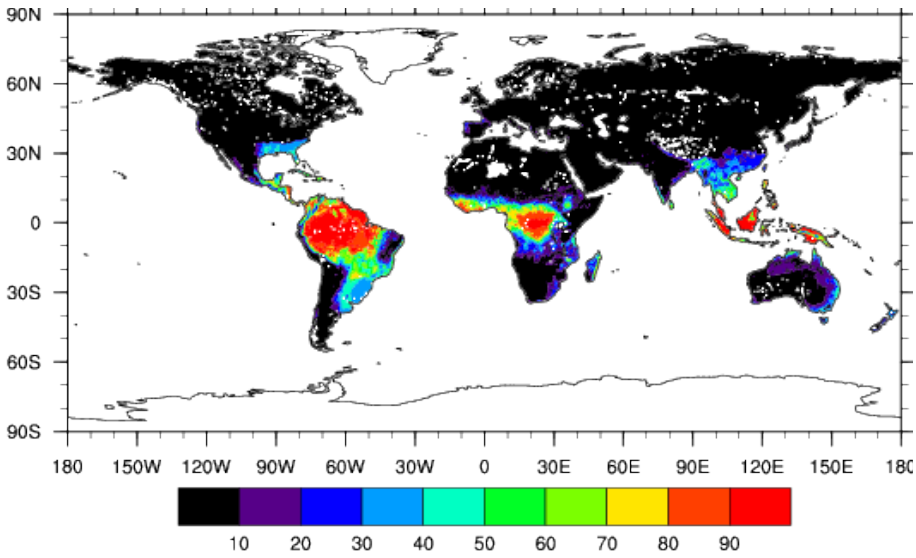


(a) Broadleaf trees millennial cover fraction (%)

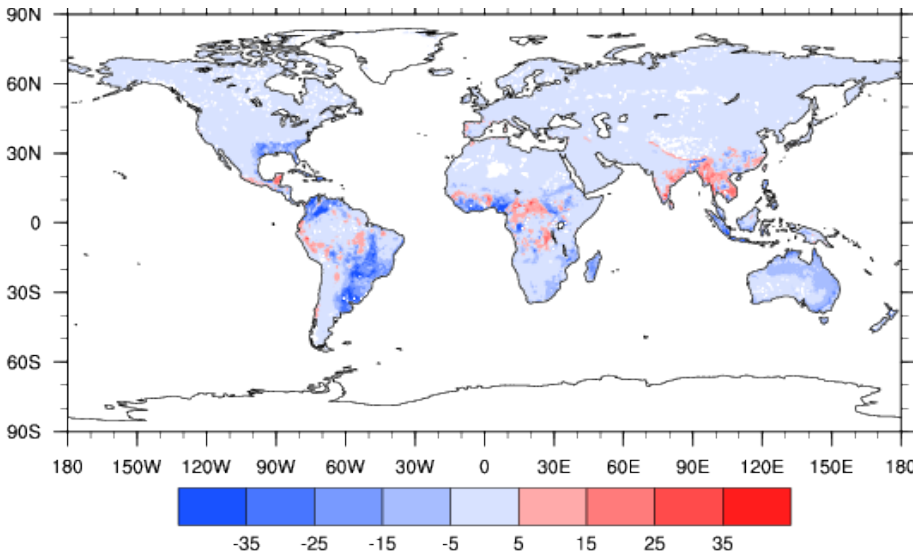


(b) Broadleaf trees cover fraction change (%)

**Figure 3.8:** (a) Broadleaf tree cover fraction (%) (1000-1990) and (b) Broadleaf tree cover fraction change (%) between 1950-1990 as compared to 1000-1800.

century loosing a large fraction of the population in times marked by famines and abandonment of agricultural land (3.11 c) (Kaplan et al., 2010).

## 3.4 Modeling of Terpenoid BVOC Emissions

Above canopy fluxes of isoprene (IP), monoterpenes (MT) and sesquiterpenes (ST) were estimated using the MEGAN algorithm in every gridbox following the general equation (Guenther et al.,

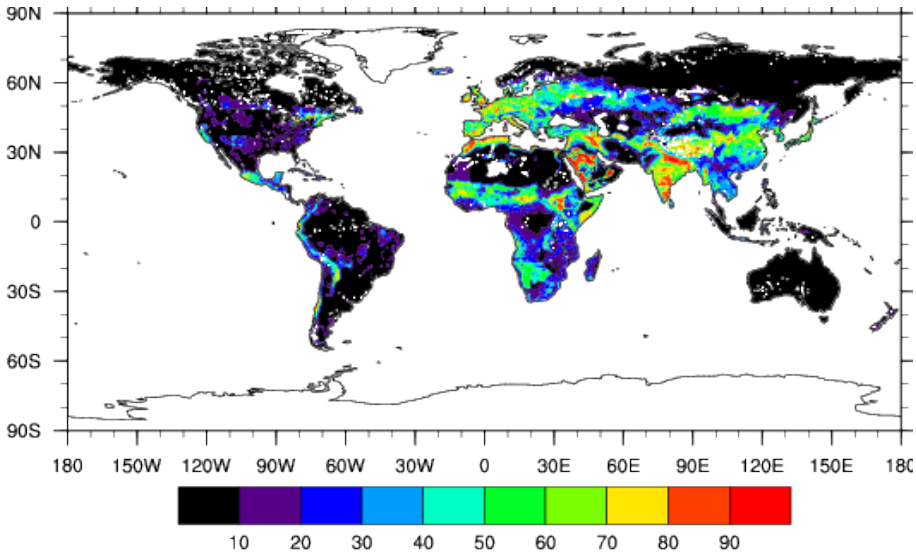


(a) Herbaceous trees millennial cover fraction (%)

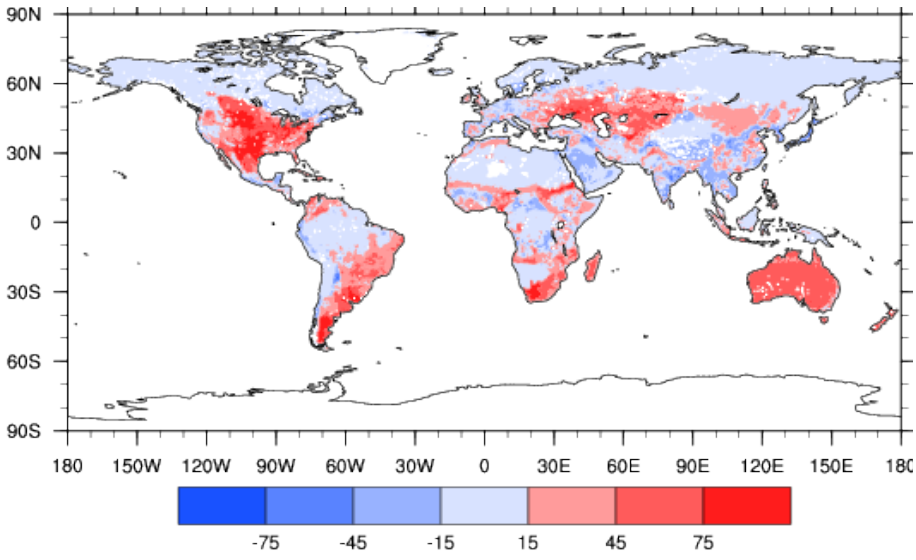


(b) Herbaceous trees cover fraction change (%)

**Figure 3.9:** (a) Herbaceous cover fraction (%) (1000-1990) and (b) Herbaceous cover fraction change (%) between 1950-1990 as compared to 1000-1800

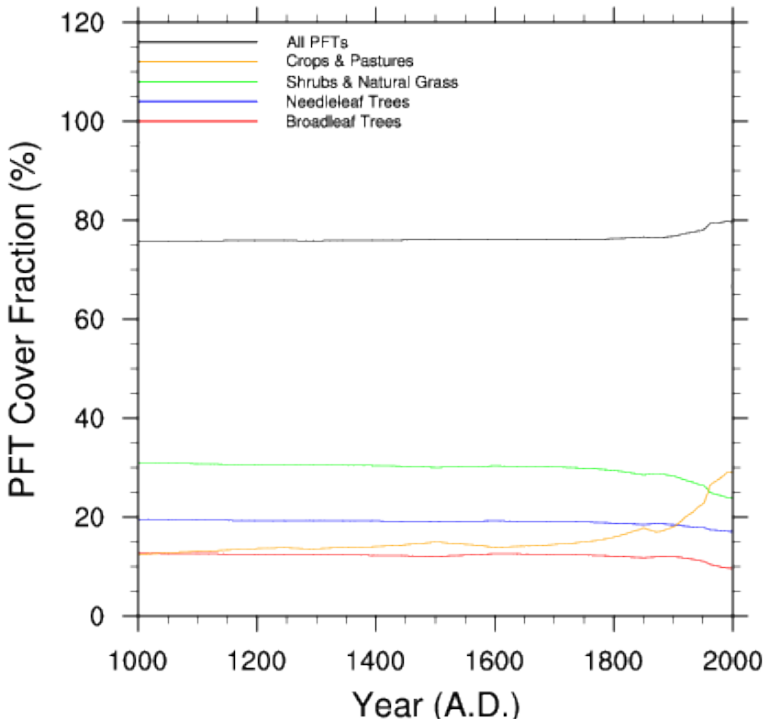


**Figure 3.10:** Time evolution of the global Plant Functional Type (PFT) area coverage (%).

2006):

$$E = \epsilon * \gamma_{LAI} * \gamma_T * \gamma_{age} * \gamma_{SM} * \gamma_{CO_2} * ((1 - LDF) + LDF * \gamma_P), \tag{3.1}$$

where $E$ (mg m$^{-2}$ h$^{-1}$) is the flux of any given BVOC and it is determined by the empirical emission activity factor $\epsilon$ (mg m$^{-2}$ h$^{-1}$) of every plant functional type (table 3.3) at standard conditions, the deviation factors from standard conditions: $\gamma_{LAI}$, $\gamma_T$, $\gamma_{age}$, $\gamma_{SM}$, $\gamma_{CO_2}$, $\gamma_P$, and a Light Dependency Factor ($LDF$) for every compound (table 3.4). The standard conditions for the MEGAN canopy-scale emission factors include a LAI of 5; canopy with 80% mature, 10% growing and 10% old foliage; a solar zenith angle of 30 deg; a photosynthetic photon flux density (PPFD) transmission of 0.6 and air temperature of 303 K. Activity factors $\gamma_{LAI}$, $\gamma_T$, $\gamma_{age}$, $\gamma_{SM}$, $\gamma_{CO_2}$, $\gamma_P$ account for changes in the emissions due to deviations from standard conditions and are determined by climate and land-cover variables.

### 3.4.1 Leaf Area Index Effect

BVOC emissions grow rapidly with increasing LAI and gradually tend to a constant asymptotic behavior for LAI larger than approximately 2.5, meaning that the emissions reach a saturation point. The LAI dependence of IP, MT and ST emissions is parametrized using:

$$\gamma_{LAI} = \frac{0.49 * (LAI)}{(1 + 0.2LAI^2)^{0.5}}. \tag{3.2}$$

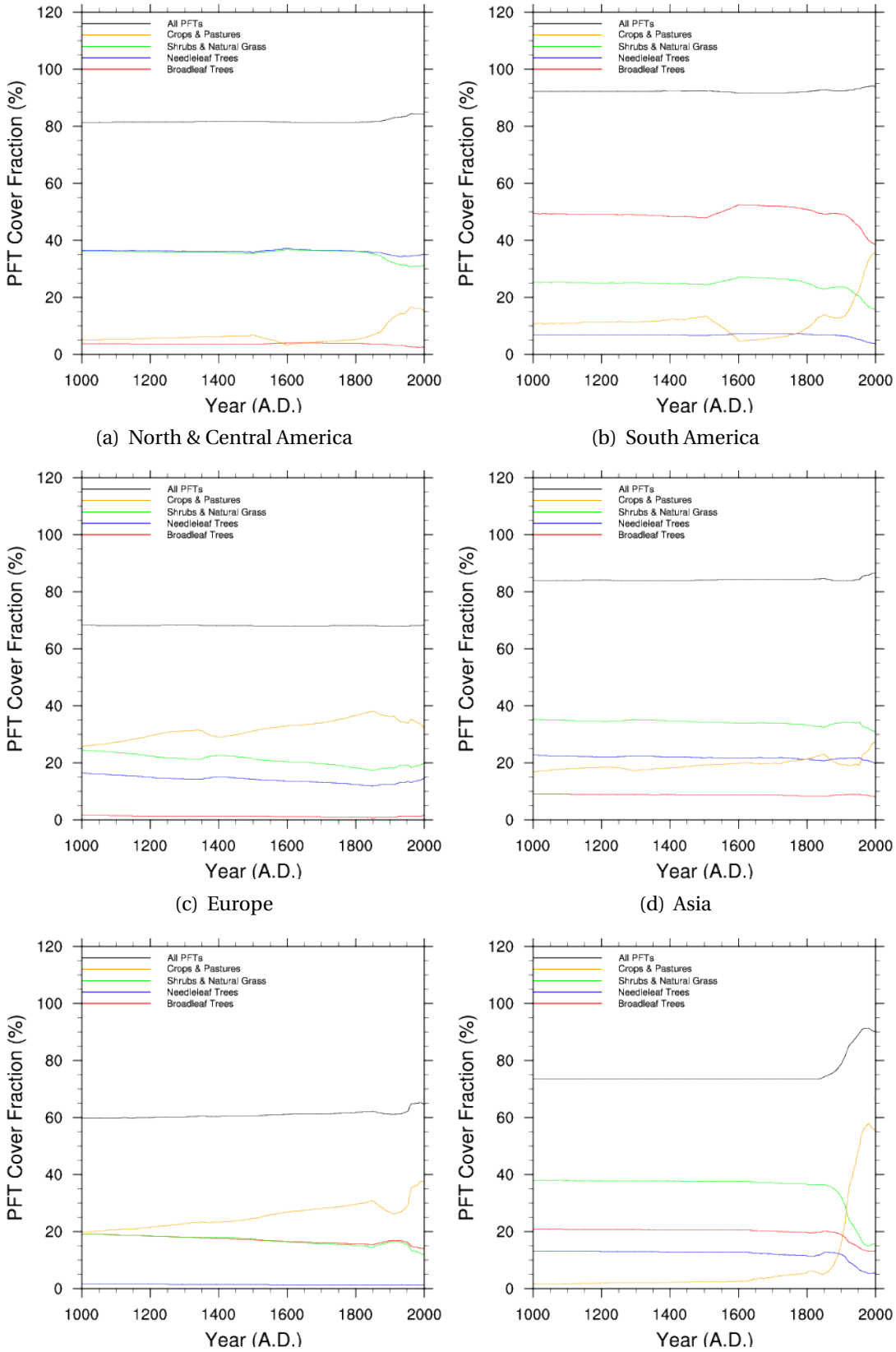


(a) North & Central America

(b) South America

(c) Europe

(d) Asia

(e) Africa

(f) Oceania

**Figure 3.11:** Time evolution of Plant Functional Type (PFT) area coverage (%) in (a) North & Central America, (b) South America, (c) Europe, (d) Asia, (e) Africa and (f) Oceania.

**Table 3.4:** Light Dependency Factor (LDF) for the calculated species.

| Compound Name | Compound Family | Light Dependency Factor (LDF) |
|---|---|---|
| Isoprene | Isoprene | 0.999 |
| Myrcene | Monoterpenes | 0.05 |
| Sabinene | Monoterpenes | 0.1 |
| Limonene | Monoterpenes | 0.05 |
| 3-Carene | Monoterpenes | 0.05 |
| $\beta$ - pinene | Monoterpenes | 0.1 |
| $\alpha$ - pinene | Monoterpenes | 0.1 |
| Other monoterpenes | Monoterpenes | 0.1 |
| $\alpha$ - farnesene | Sesquiterpenes | 0.5 |
| $\beta$ - caryophyllene | Sesquiterpenes | 0.5 |
| Other sesquiterpenes | Sesquiterpenes | 0.5 |

### 3.4.2 Surface Air Temperature Effect

The factor $\gamma_T$ accounts for the leaf temperature effect on emissions, IP emissions grow exponentially with temperature until they reach a saturation temperature after which the emissions start to decrease. IP emitting plants response to temperature is described by:

$$\gamma_T = \frac{E_{opt} * C_{T2} * exp(C_{T1} * x)}{[C_{T2} - C_{T1} * (1 - exp(C_{T2} * x))]}, \tag{3.3}$$

where $x = [(1/T_{opt}) - (1/T_{hr})]/0.00831$, $E_{opt} = 1.75 * exp(0.08(T_{daily} - 297)$, $C_{T1} = 80$, $C_{T2} = 200$, $T_{hr}$ is the hourly average SAT, $T_{daily}$ is the daily average SAT and $T_{opt} = 313 + 0.6(T_{daily} - 297)$. MT and ST emissions grow exponentially with increasing leaf temperature, MT and ST emitting plants response follows:

$$\gamma_T = exp[\beta * (T - T_s)], \tag{3.4}$$

where $\beta$ is a temperature dependent parameter and $T_s = 303$°K.

### 3.4.3 Leaf Age Effect

The factor $\gamma_{age}$ describes the effect of leaf aging of BVOC emitting species and its effect on emission activity following:

$$\gamma_{age} = F_{new} * A_{new} + F_{gro} * A_{gro} + F_{mat} * A_{mat} + F_{old} * A_{old}, \tag{3.5}$$

where $F_{new}$ is the new foliage fraction, $F_{gro}$ is the growing foliage fraction, $F_{mat}$ is the mature foliage fraction, $F_{old}$ is the old foliage fraction, $A_{new}$ is the relative emission activity for new foliage, $A_{gro}$ is the relative emission activity for growing foliage, $A_{mat}$ is the relative emission activity

for mature foliage and $A_{old}$ is the relative emission activity for old foliage. There are 3 cases for calculating the foliage fraction F, they depend on the monthly LAI change as characterized by current LAI conditions ($LAIc$) and past month's LAI conditions ($LAIp$):

1. $LAIc = LAIp$
   $F_{new} = 0.0$ , $F_{gro} = 0.1$ , $F_{mat} = 0.8$ , $F_{old} = 0.1$

2. $LAIp > LAIc$
   $F_{new} = 0.0$ , $F_{gro} = 0.0$, $F_{mat} = 1 - F_{old}$, $F_{old} = (LAIp - LAIc)/LAIp$

3. $LAIp < LAIc$
   $F_{new} = 1-(LAIp/LAIc)$, $F_{mat} = LAIp/LAIc$, $t <= ti$
   $F_{new} = (ti/t) * (1 - (LAIp/LAIc))$, $F_{mat} = (LAIp/LAIc) + ((t - tm)/t) * (1 - (LAIp/LAIc))$, $t > ti$
   $F_{gro} = 1 - F_{new} - F_{mat}$, $F_{old} = 0.0$.

Where $t_i = 5 + (0.7 * (300 - T_t))$ if $T_t <= 303°$K and $t_i = 2.9$, if $T_t > 303°$K. $t_i$ is the number of days between budbreak and the induction of emission, $t_m = 2.3 * t_i$, $t$ is the length of the time step in days, $t_m$ is the number of days between budbreak and the initiation of peak emissions rates and $T_t$ is the average temperature near top of the canopy during current time period (average SAT).

There are 3 cases for relative emission activity A:

1. Isoprene
   $A_{new} = 0.05$, $A_{gro} = 0.6$, $A_{mat} = 1.125$, $A_{old} = 1.0$

2. Monoterpenes
   $A_{new} = 2.0$, $A_{gro} = 1.8$, $A_{mat} = 0.95$, $A_{old} = 1.0$

3. Sesquiterpenes
   $A_{new} = 0.4$, $A_{gro} = 0.6$, $A_{mat} = 1.075$, $A_{old} = 1.0$

### 3.4.4 Soil Water Content Effect

The factor $\gamma_{SW}$ describes the IP emitting plants response to drought by decreasing the cell enzymatic activity due to a shortage of water. The activity is estimated by comparing MPI-ESM monthly average fields of Soil Water (SW) content in $m^3\ m^{-3}$ with MEGAN averaged Wilting Point

(WP) in the top and bottom layers of the soil. If the SW is lower than the WP, the plants cannot extract water from the soil and the emissions are interrupted, resembling the conditions during drought. $\gamma_{SW}$ is parametrized as:

$$\begin{aligned} \gamma_{SW} &= 0, && SW \leq WP \\ \gamma_{SW} &= \frac{SW - WP}{\delta SM}, && WP < SM \leq WP + \delta SM \\ \gamma_{SW} &= 1, && SW > WP + \delta SM, \end{aligned} \tag{3.6}$$

where $\delta SM$ = 0.06 and WP depends on the specific soil type for a given location.

### 3.4.5 Carbon Dioxide Effect

Isoprene (IP) emissions from plants decrease with increasing carbon dioxide concentrations as supported by several studies summarized in Penuelas et al. (2010), this response is parametrized following Guenther et al. (2012):

$$\gamma_{CO_2} = IS_{max} - \frac{IS_{max} * C_i^h}{C_{star}^h + C_i^h} \tag{3.7}$$

Parameters $IS_{max}$ = 1.344, $h$ = 1.4614, $C_{star}$ = 585 and $C_i$ = 0.7* [$CO_2$] are estimated empirically. $\gamma_{CO_2}$ has a value of 1 when $CO_2$ concentrations are 400 ppmv. MT and ST emissions are not parametrized as a function of $CO_2$ in our simulations due to the lack of scientific evidence linking a clear effect (Peñuelas et al., 2010).

### 3.4.6 Solar Radiation Effect

Solar radiation in the 400-700nm wavelength range drives the plant cellular activity associated with the production of terpenoid BVOC. BVOC species emitted after synthesis are more sensitive to light than species emitted from storage pools. The LDF factors used are displayed in table 3.4. Photosynthetically available radiation (PAR) is converted to Photosynthetic Photon Flux Density (PPFD) and its effect on IP, MT and ST emissions is described by:

$$\gamma_P = sin(\theta) * [2.46 * (1 + 0.0005(P_{daily} - 400)) * \phi - 0.9 * \phi^2], \tag{3.8}$$

where $\theta$ is the solar angle in degrees, $\phi = P_{ac}/(sin(\theta) * P_{toa})$ is the above canopy PPFD transmission, $P_{ac}$ = DSRS * 0.5 * 4.766 $\mu$mol m $^{-2}$s$^{-1}$ is the hourly PPFD value above canopy, $P_{toa}$ = $3000 + 99 * cos[2 * 3.14 - (DOY - 10)/365)]$ is the PPFD value at the top of atmosphere, $DOY$ is

the day of year and $P_{daily}$ is the daily average of $P_{ac}$.

## 3.5 Setup

1. **Climate data preprocessing**: The data provided by MPI-ESM for the time period between years 1000 to 1990 AD includes global values for SAT, DSRS, LAI and SW. The daily averages with a spatial resolution of 3.75° x 3.75° were used. Rather strict file standards are required to compile MEGAN, the raw climate data was modified to conform to these standards by merging independent netcdf files for each climate variable into a common netcdf file. Global attributes describing the conditions of the model (grid description, starting dates, data timesteps, etc.) needed to be created and added to the merged file. A new variable describing the model output times was also added to the final file.

2. **Land-Use data preprocessing**: PFT distributions on the surface of the earth were provided for the modeled period. A space resolution compatible with MEGAN was necessary so the original files were regridded from 0.5° x 0.5° to 3.75° x 3.75°. A .csv file was created and converted to a compatible netcdf file using software supplied with MEGAN. The netcdf file containing all PFT values was re-gridded into the resolution of MEGAN using cdo (cdf operators) software.

3. **Model modifications**: The default model reads in climate information at every model time-step (3 hours). A major change was to parametrize the diurnal cycles in radiation and temperature. The radiation fields were scaled with the solar zenith angle. The scaling coefficient depends on latitude and the day of the year and ensures the daily average radiation from the parametrization equals the daily average from the MPI-ESM model output. Daily SAT variations were estimated using the daily minimum and maximum temperatures from the MPI-ESM model and the parametrization of a daily SAT, where daytime SAT follows a sinusoidal function and nighttime SAT follow a negative exponential function. A complete description of the parametrization is described by Parton (1981).

## 3.6 Millennial Simulations

MEGAN was driven off-line in a series of 10 different simulations. Simulations 1-5 described in table 3.5 were carried out to test emission sensitivity to SAT, DSRS and SW fields from MPI-ESM simulations with all natural and anthropogenic forcings **OFF**. SAT daily cycle parameterization (Parton, 1980), Dynamic Vegetation (DV), Soil Water (SW) content parametrization and carbon dioxide parameterization were added one at a time to evaluate the individual effects

**Table 3.5:** Description of the 10 different simulated scenarios. The first 5 simulations for IP (3 for MT and ST) were done by driving MEGAN with a controlled MPI-ESM simulation to test individual sensitivities of the model to different parameters. The last 5 simulations were done forcing MEGAN with a full forcing millennial simulation of MPI-ESM and adding the effects progressively to reach the most realistic scenario (No. 10 for IP and No. 8 for MT and ST.

| Simulation ID | Natural + Anthrop. Climate Forcings | SAT Daily Cycle Parametrization | Dynamic Vegetation | Soil Moisture | Carbon Dioxide Concentration |
|---|---|---|---|---|---|
| 1 | Off | Off | Off | Off | Off |
| 2 | Off | **On** | Off | Off | Off |
| 3 | Off | Off | **On** | Off | Off |
| 4 | Off | Off | Off | **On** | Off |
| 5 | Off | Off | Off | Off | **On** |
| 6 | **On** | Off | Off | Off | Off |
| 7 | **On** | **On** | Off | Off | Off |
| 8 | **On** | **On** | **On** | Off | Off |
| 9 | **On** | **On** | **On** | **On** | Off |
| 10 | **On** | **On** | **On** | **On** | **On** |

separately. Simulations 6-10 described in table 3.5 were carried out to test emission variability due to variability of SAT, DSRS and SW fields from MPI-ESM simulations with all natural and anthropogenic forcings **ON**. SAT parameterization, Dynamic Vegetation (DV), Soil Water (SW) content parametrization and carbon dioxide parameterization were added progressively to build up the most realistic scenario by steps. For simplicity, we refer to simulations 1-5 as controlled simulations and 6-10 as full forcing simulations. It is important to note that parameterization of SW and $CO_2$ concentration were not applied to MT and ST emissions because there is no concluding scientific evidence linking the change in emissions of MT and ST due to those individual effects. This means that results from runs 4, 5, 9 and 10 are only IP emission results.

# 4

# Results and Discussion

## 4.1 Regional and Seasonal Variability of Terpenoid BVOC Emissions

### 4.1.1 Isoprene

The results of IP emissions in simulation # 10 (See table 3.5) with all effects included are presented in figure 4.1. A map of the global averaged (1000-1990) emissions of IP is shown in figure 4.1 a. IP emissions are dominant in the tropics and subtropics due to the presence of high emitting vegetation, elevated yearly mean temperature and solar radiation. Over tropical rainforest yearly mean emissions range from 50 to 100 mg $m^{-2}$ $d^{-1}$, while over boreal zones the values are less than 1 mg $m^{-2}$ $h^{-1}$. Mid-latitude and boreal vegetation emissions vary largely over season, during summer values can be as large as 30 mg $m^{-2}$ $d^{-1}$, while winter averages are close to zero (4.1 a, 4.3).

The average emission change between the periods 1000-1800 and 1950-1990 are shown in figure 4.1 b. A reduction ranging from 0 to over 75% is observed over regions in central North America, southern South America, central Eurasia and northern Australia due to the combination of cropland expansion and the $CO_2$ concentration effects. Above South American, African, Asian rainforests and boreal forests the temperature effect dominates resulting in higher emissions ranging from 0 to 50% at some locations.

In South America, expanding anthropogenic vegetation with low IP emitting rates (crops + pastures) replaced high emitting local vegetation (Broadleaf trees) in the southeast leading to a reduction of 5 to 75 % depending on location (Blue region in figure 4.1 b). In contrast, the vegetation unaltered by humans in the Amazon region responded to SAT change with an increment in the emissions between 5 and in a few locations up to more than 75 % (Red region in figure 4.1

b). A shift in the emission pattern with rising emissions of IP in the northern South America and a reduction in the south is predicted by our model by the combined effect of land-use and SAT changes. The total averaged emissions in South America decreased from about 300 Tg $yr^{-1}$ to 265 Tg $yr^{-1}$ from preindustrial to present day (blue solid line of figure 4.2. South America contributes to about a half of the total global IP emissions because it has the largest tropical rain forest in the world.

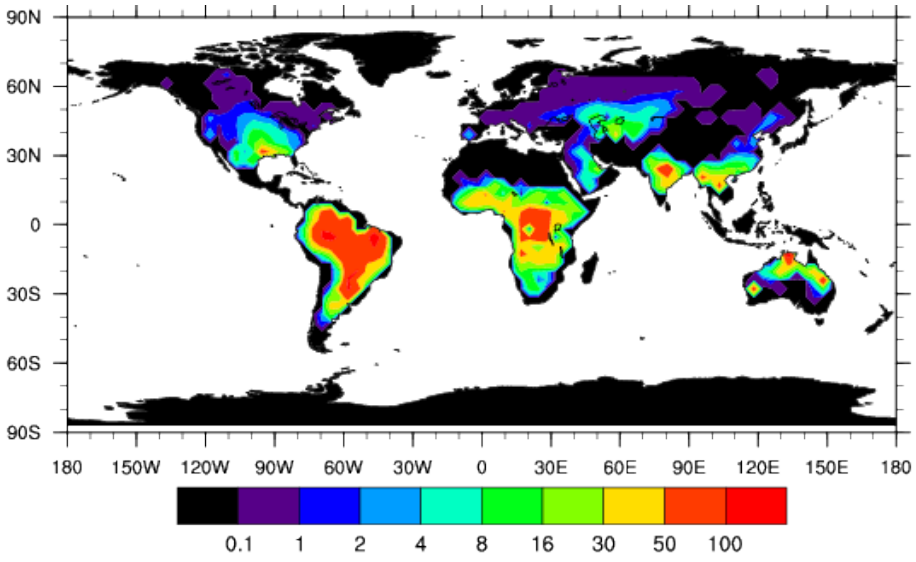


(a) IP mean millennial emissions (mg $m^{-2}$ $d^{-1}$)

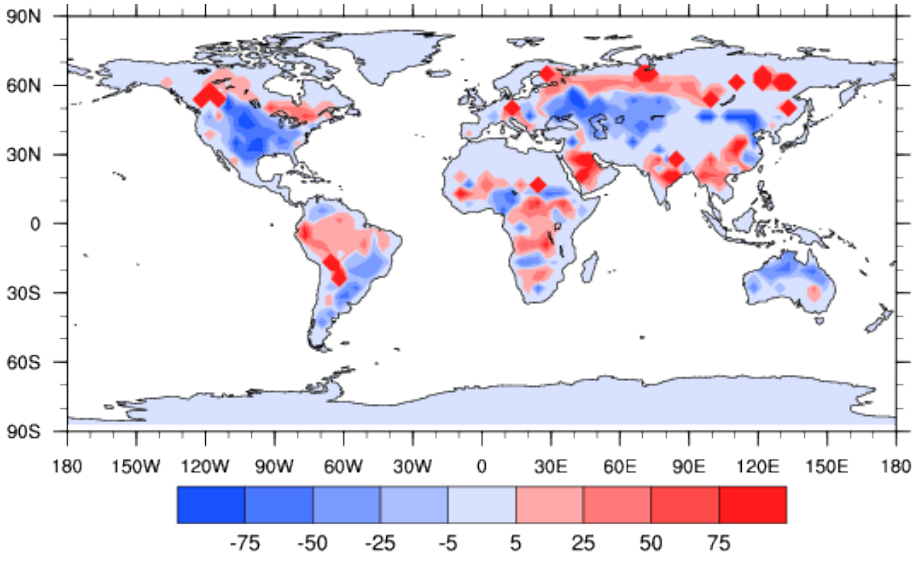


(b) Mean IP emission change (%)

**Figure 4.1:** (a) IP mean millennial emissions and (b) Mean IP emission change between 1000-1800 and 1950-1990 for simulation # 10.

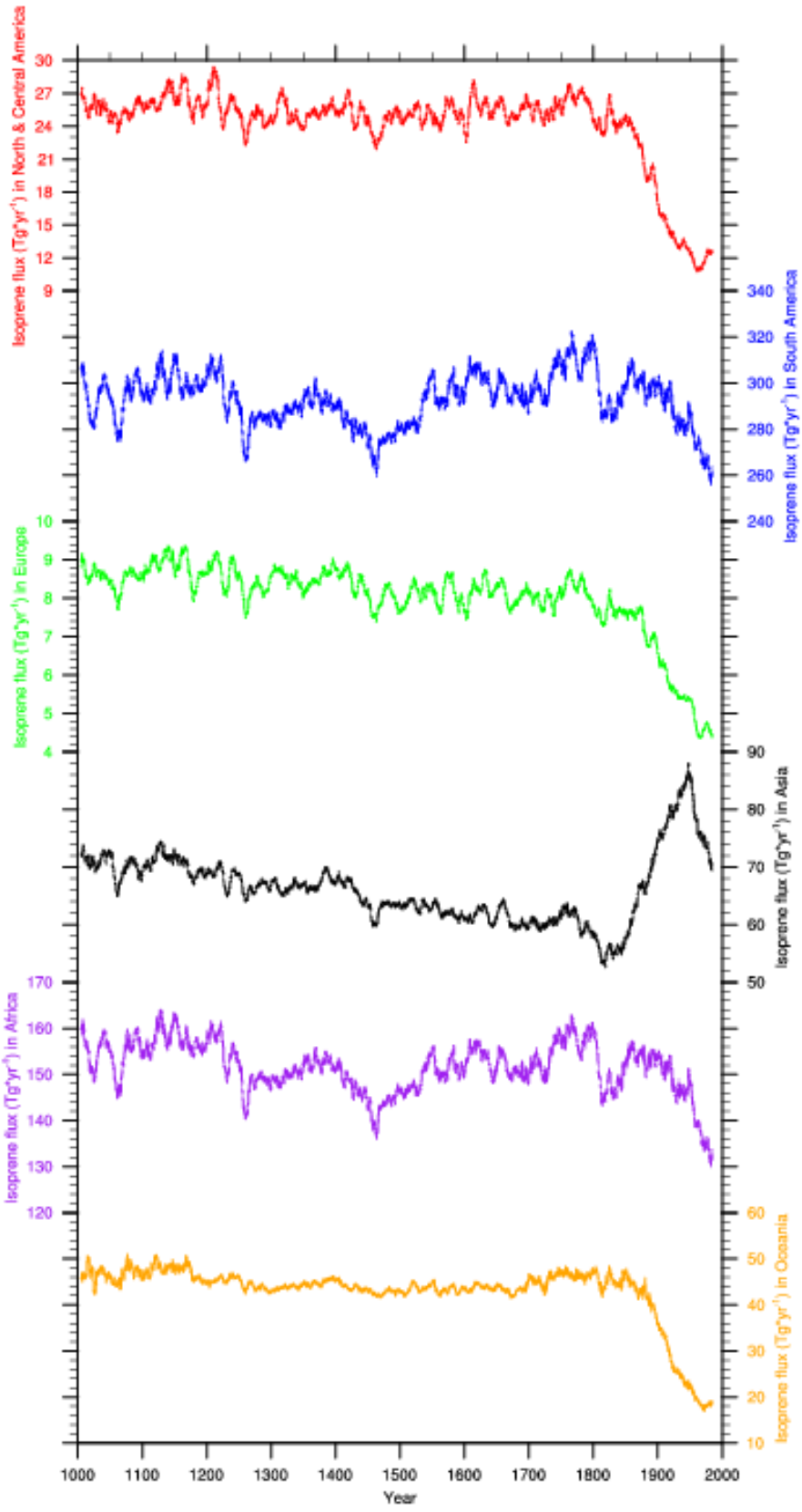


**Figure 4.2:** IP regional millennial emissions (simul. # 10).

A significant fraction of the African continent is covered by tropical rain forest, making it an important source of the IP, approximately one forth of the global IP emissions are originated in Africa. Similar to South America, African IP global emission change is regional dependent. Virgin tropical rain forest emits larger amounts of IP nowadays than before preindustrial times (Red zones in figure 4.1 b) due to SAT anomalies, but regions where either, natural shrub and broadleaf trees have disappeared to give way to plantations and pastures show a significant loss of the IP exchange between vegetation and atmosphere (blue zones in figure 4.1 b). The reduction of IP emissions occurs in Africa where preindustrial and present day values are 150 Tg $yr^{-1}$ and 140 Tg $yr^{-1}$ respectively (purple solid line of figure 4.2).

Vast regions in North America and Oceania have suffered a severe transformation due to the shifts in the use of land. High IP emitting species have given way to crops and pastures resulting in an important reduction of the total IP emissions throughout the millennium (Blue regions in figure 4.1 b). Total emissions are reduced from 45 Tg $yr^{-1}$ to 20 Tg $yr^{-1}$ in Oceania and from 25 g $yr^{-1}$ to 13 Tg $yr^{-1}$ in North and Central America (Yellow and red solid lines of figure 4.2). A similar land-use effect is observed in central Eurasia, causing European emissions to decrease from 8 Tg $yr^{-1}$ to 5 Tg $yr^{-1}$ (Green solid line of figure 4.2). The total Asian emissions are, in contrast, dominated by an enhancing effect of IP emissions in southeast Asia, the Indian sub-continent and regions in the middle East (Red regions in figure 4.1 b) due to rising SAT and the practice of agriculture in former non-vegetated lands. As a result, Asian emissions increase from 65 Tg $yr^{-1}$ to 72 Tg $yr^{-1}$ (Black solid line of figure 4.2).

The seasonal emission distribution which is shown in figure 4.3, indicates that monthly IP emissions vary over season. Total global emissions are higher during the boreal summer indicating that IP emitting vegetation contribution to the global emissions during the growing season is larger in the northern hemisphere than in the southern hemisphere. Global emissions vary from a minimum value of 500 Tg $yr^{-1}$ in November to a maximum of 800 Tg $yr^{-1}$ in August (Figure 4.3 e).

Figure 4.4 displays the percent distribution of IP emissions averaged from 1000-1800 and b from 1950-1990 showing only a significant reduction in North American and Oceania emissions. South American emissions account for approximately half of the total global emissions changing after preindustrial times from 49.8% to 52%, African emissions represent around one forth varying from 25.8% to 26.5%, while Asian emissions increase from 11.1% to 14.7%, North and Central American emissions decrease from 4.3% to 2.2%, European emissions are reduced from 1.4% to 0.9% and emissions over Oceania decrease from 7.6% to 3.7%.

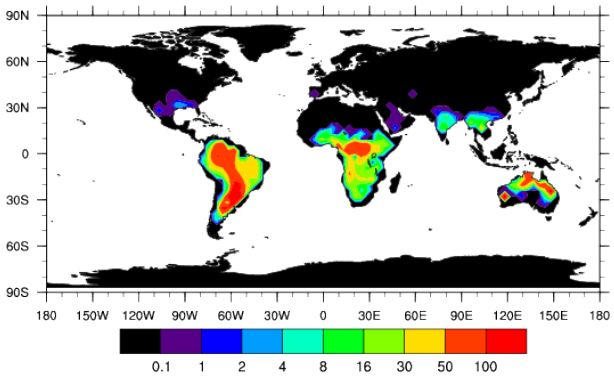


(a) Mean January IP millennial emissions (mg $m^{-2}$ $d^{-1}$)

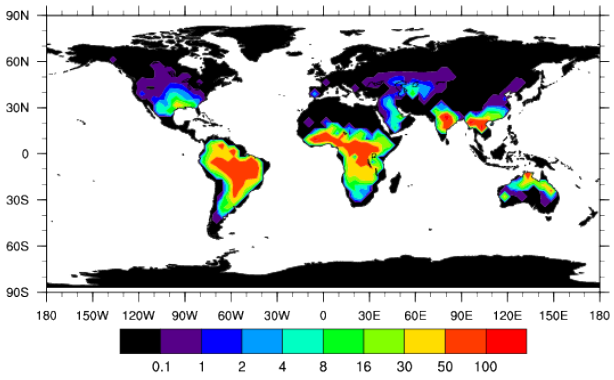


(b) Mean April IP millennial emissions (mg $m^{-2}$ $d^{-1}$)

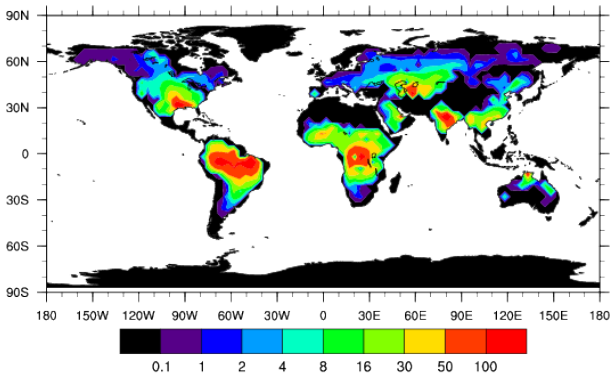


(c) Mean July IP millennial emissions (mg $m^{-2}$ $d^{-1}$)

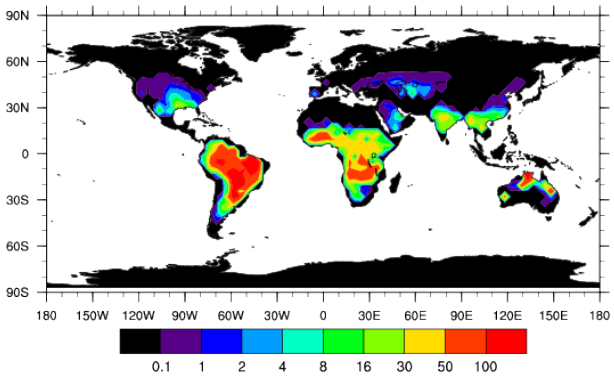


(d) Mean October IP millennial emissions (mg $m^{-2}$ $d^{-1}$)

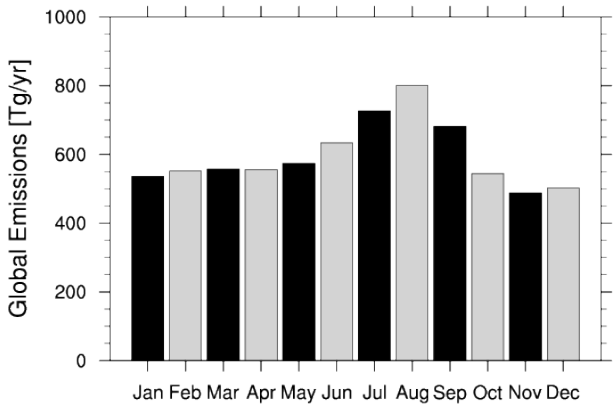


(e) Monthly IP emissions

**Figure 4.3:** Mean IP millennial emissions in (a) January, (b) April, (c) July, (d) October and (e) total monthly emissions for simulation # 10.


(a) Regional IP 1000-1800 emission distribution

(b) Regional IP 1950-1990 emission distribution

**Figure 4.4:** (a) Regional IP 1000-1800 emission distribution and (b) regional IP 1950-1990 emission distribution for simulation # 8.

### 4.1.2 Monoterpenes

The best estimate (simulation # 8 in table 3.5) of MT emissions are presented in figure 4.5. Tropical and sub-tropical vegetation are the largest contributors of MT emissions with yearly averages of 5 to 10 mg $m^{-2}$ $d^{-1}$, an order of magnitude less than IP emissions for the same regions (Figure 4.5 a). The case is different over boreal forest where yearly mean MT emissions can be as high as 1 mg $m^{-2}$ $d^{-1}$, values in the same order of magnitude as IP. The model predicts a clear seasonal dependence of MT emissions in mid and high- latitude locations, where emissions can vary from 5 mg $m^{-2}$ $d^{-1}$ during summer to no emissions in wintertime (Figure 4.7).

In contrast to IP, calculated MT emissions increase systematically from preindustrial to present times in every region with a few exceptions in central North America, southeastern South America, eastern Australia and central Eurasia (Blue regions figure 4.5 b). A strong deforestation at this locations where natural shrubs were the dominant species was followed by a gradual shift in the use of land due to agricultural practices where species with lower MT emission rates replaced the natural vegetation (Table 3.3). The increment in MT emissions ranges between 5-25% in most locations driven by temperature anomalies (light red regions) and replacement of natural vegetation with crops or pastures that have similar MT emission rates than the existing vegetation before the changes induced by humans (Table 3.3). In mid-western USA, western Australia and a few regions in central Asia the MT emissions change rises up to more than 75% due to colonization and development of agriculture in locations where natural vegetation was previously scarce (dark red regions figure 4.5) b). Local shifts in emissions occur over time with a small overall effect in North America due to a reduction of emissions in the mid-eastern area and an increase elsewhere. Similarly, Eurasian emissions decrease in a few particular mid-latitude regions and increase in the rest of the continent. Australian emissions shift west but follow the mean global temperature,

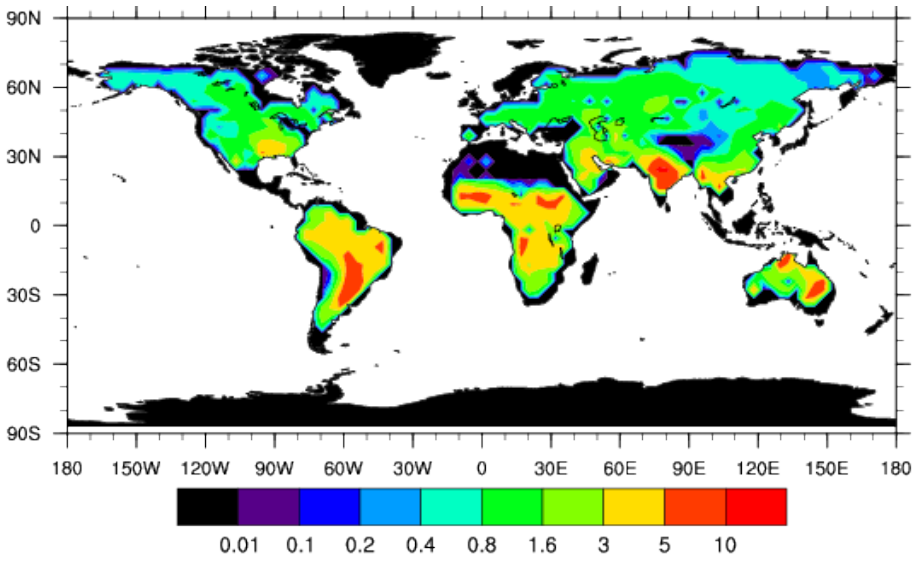


(a) MT mean millennial emissions (mg $m^{-2}$ $d^{-1}$)

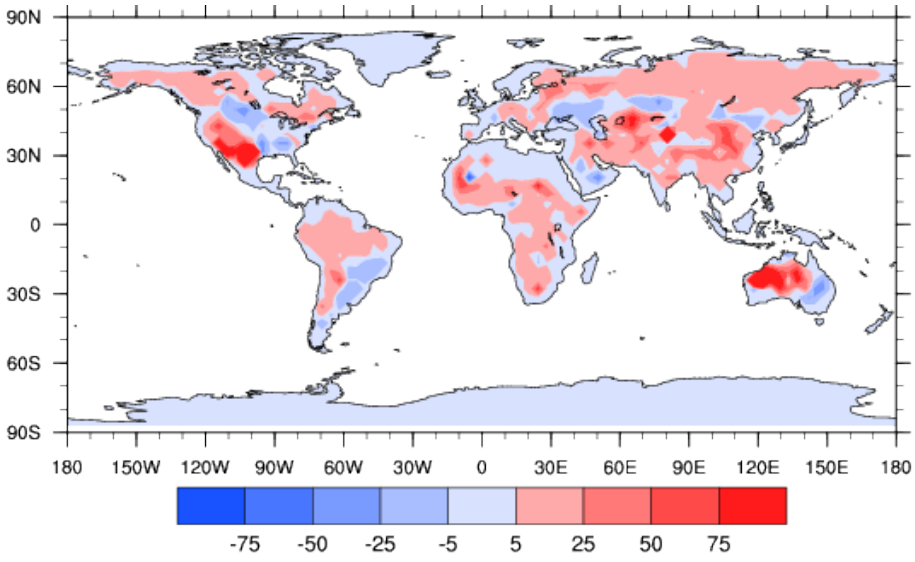


(b) Mean MT emission change (%)

**Figure 4.5:** (a) MT mean millennial emissions and (b) Mean MT emission change between 1000-1800 and 1950-1990 for simulation # 8.

like Central and North American, European, Asian and African emissions.

Figure 4.6 displays the regional millennial evolution of MT emissions. The estimated total regional emissions show a similar overall response to rising SAT in every region except South America where MT emissions increase over virgin forests driven by SAT changes, while over the south-eastern plains MT emissions are controlled by land-use change. South American emissions show a high temporal variability but keep a rather fixed mean annual emissions of 17.5 Tg $yr^{-1}$

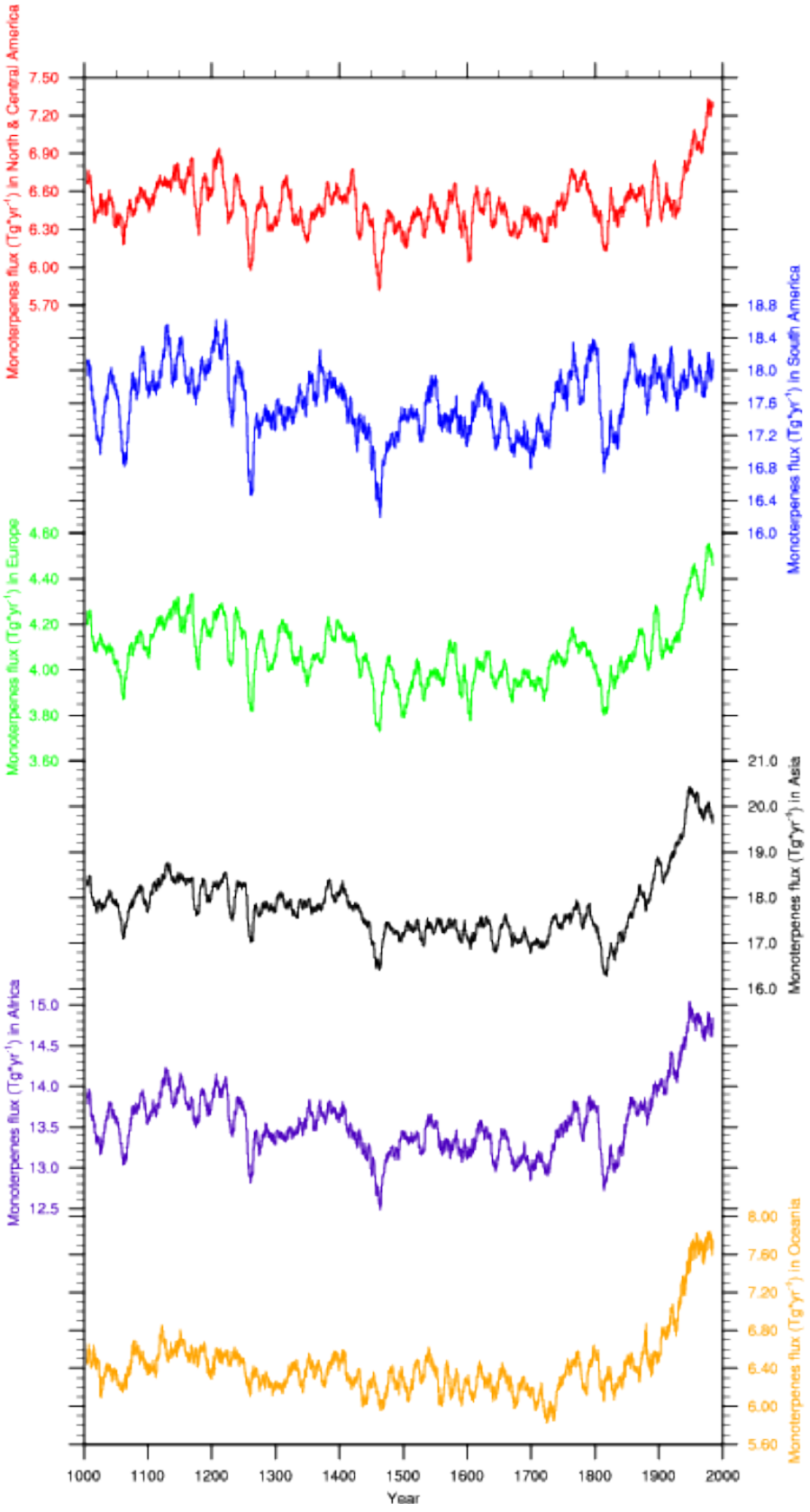


**Figure 4.6:** MT regional millennial emissions (simul. # 8).

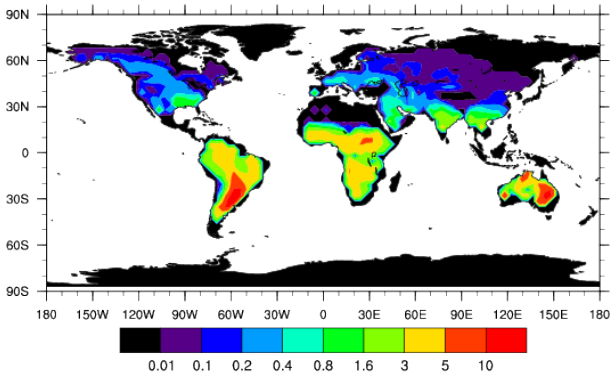


(a) Mean January MT emissions (1000-1990)

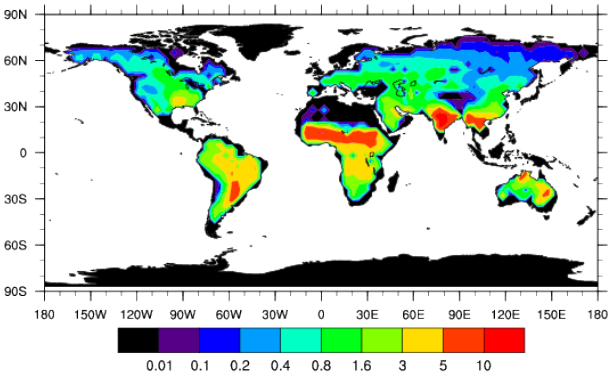


(b) Mean April MT emissions (1000-1990)

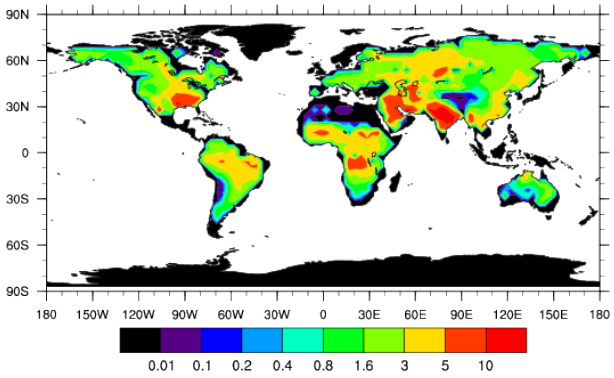


(c) Mean July MT emissions (1000-1990)

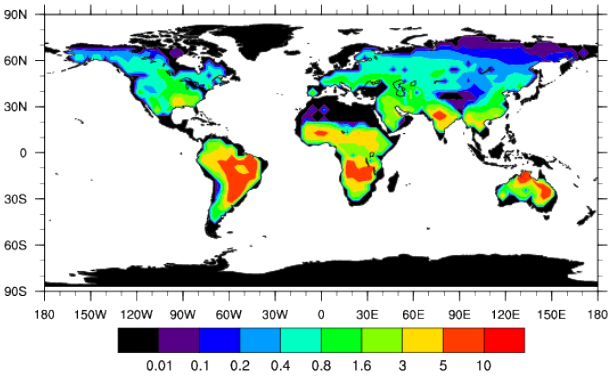


(d) Mean October MT emissions (1000-1990)

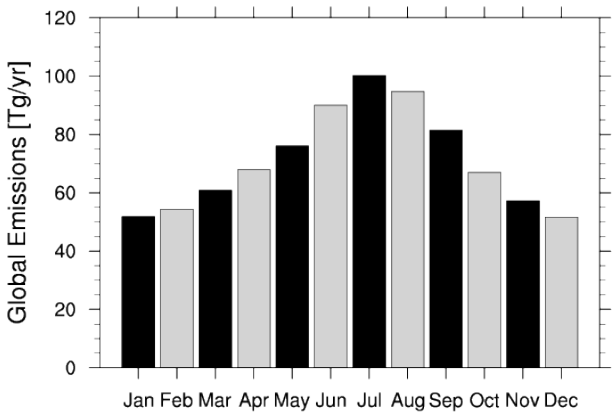


(e) Seasonality of MT emission (1000-1990)

**Figure 4.7:** Mean MT millennial emissions in (a) January, (b) April, (c) July, (d) October and (e) total monthly emissions for simulation # 8.


(a) Regional MT 1000-1800 emission distribution

(b) Regional MT 1950-1990 emission distribution

**Figure 4.8:** (a) Regional MT 1000-1800 emission distribution and (b) regional MT 1950-1990 emission distribution for simulation # 8.

during the whole millennium explained only by a shift to the north in the emission patterns, the amount corresponds to 26.8% before 1800 and 24.9% after 1950 (Figures 4.8 a and b. North and Central American emissions grow from preindustrial (6.6 Tg $yr^{-1}$) to present day (7.1 Tg $yr^{-1}$) and represent a tenth of the total global emissions, European emissions vary from 4.1 Tg $yr^{-1}$ (6.2%) to 4.5 Tg $yr^{-1}$ (6.2%), Asian emissions change from 17.5 Tg $yr^{-1}$ (27.8%) to 20 Tg $yr^{-1}$ (26.9%), African emissions change from 13.5 Tg $yr^{-1}$ (20.5%) to 14.7 Tg $yr^{-1}$ (20.6%) and emissions over Oceania vary from 6.3 Tg $yr^{-1}$ (9.7%) to 7.6 Tg $yr^{-1}$ (10.7%).

The behavior of the mean global MT emissions during 1000-1990 is highly dependent on the season (Figure 4.7). A minimum occurs during boreal winter with values close to 50 Tg $yr^{-1}$ and a maximum during July when emissions rise to 100 Tg $yr^{-1}$ explained by a high biological activity of northern mid- and high-latitude vegetation releasing large amounts of MT into the atmosphere. Figures 4.8 a and b indicate that the regional distribution of MT emissions stays practically fixed in both periods, preindustrial and present-day.

### 4.1.3 Sesquiterpenes

Sesquiterpene (ST) emissions under simulation # 8 conditions are presented in figure 4.9 (See table 3.5). Like IP and MT, ST emissions from tropical and sub-tropical vegetation dominate the global emissions with yearly averages of around 1 mg $m^{-2}$ $h^{-1}$, an order of magnitude less than MT emissions an two lower than IP for the same regions. Over boreal forests, yearly averaged emissions are close to 0.1 mg $m^{-2}$ $d^{-1}$ and vary between 0.1 mg $m^{-2}$ $d^{-1}$ and 0.5 mg $m^{-2}$ $d^{-1}$ in mid-latitudes (Figure 4.9 a). In the same fashion as MT, ST emissions increase from preindustrial to present times in most regions. Exceptions occur in North and South America, Australia and central Eurasia (Figure 4.9 b). The increment in ST emissions ranges between 5-50% in most

locations driven by temperature anomalies, except for mid-western USA, western Australia and a few regions in central Asia where the emission' change rises up to more than 75%.

Figure 4.10 indicates that the regional evolution of ST emissions resembles the evolution of MT emissions for all regions for analogous reasons. In every continent the ST emissions increase after preindustrial times, except in South America where the emissions stayed fixed throughout the millennium. Global mean ST emissions during 1000-1990 follow a very similar seasonal

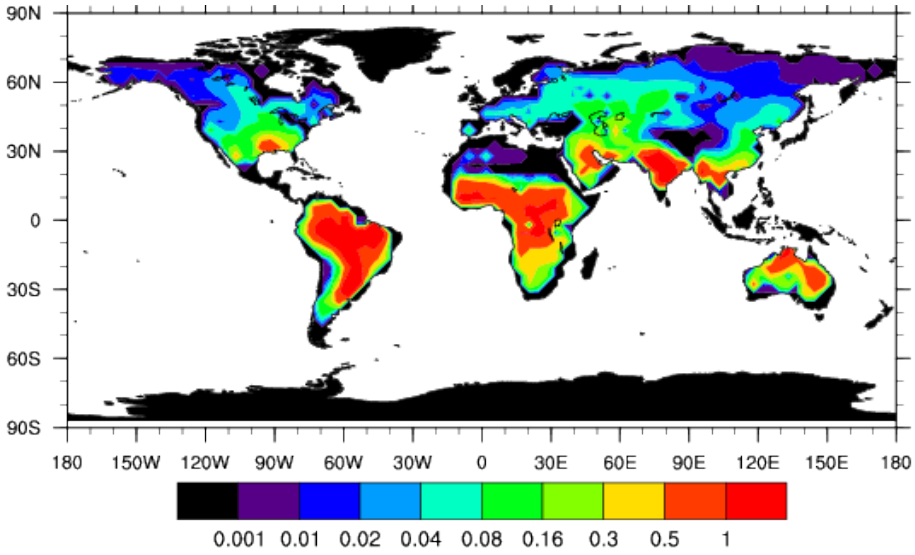


(a) ST mean millennial emissions (mg $m^{-2}$ $d^{-1}$)

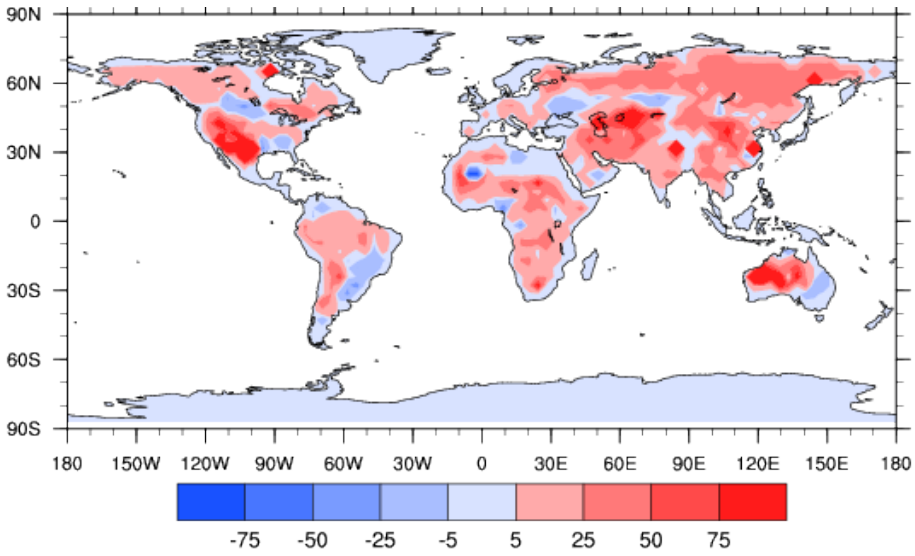


(b) Mean ST emission change (%)

**Figure 4.9:** (a) ST mean millennial emissions and (b) Mean ST emission change between 1000-1800 and 1950-1990 for simulation # 8.

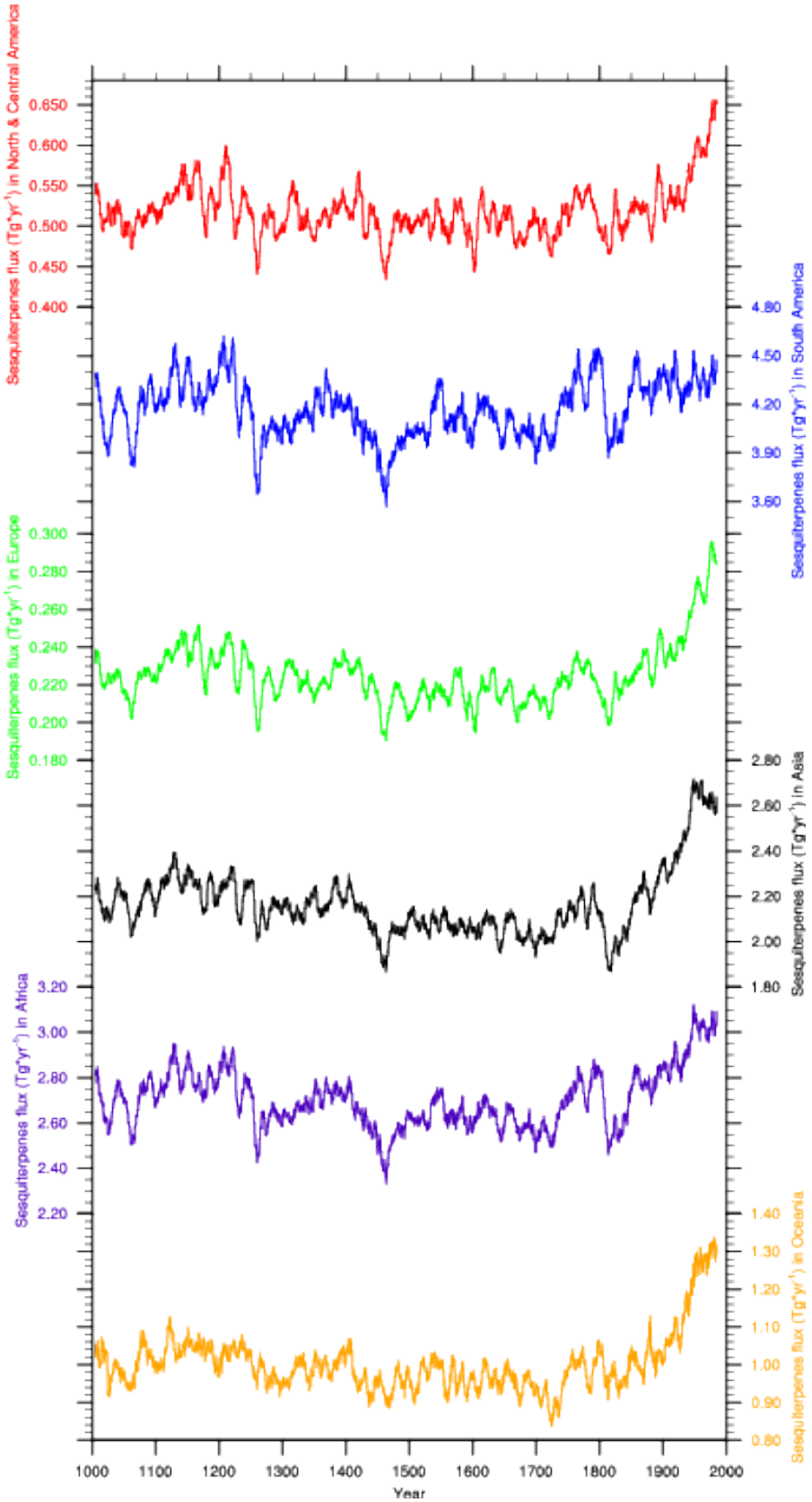


**Figure 4.10:** ST regional millennial emissions (simul. # 8).

pattern than MT, the emissions are highly dependent on the season (Figure 4.11). A minimum occurs during boreal winter with values close to 9 Tg $yr^{-1}$ and a maximum during July when emissions rise to 16 Tg $yr^{-1}$. Regional percent contribution to total ST emissions are distributed similarly from preindustrial to present day. South America emits over a third of the total global emissions, Africa emits annually one forth, Asia one fifth, Oceania one tenth, North America emits 5% and Europe emits approximately 2 % (Figures 4.12 a and b).

## 4.2 Sensitivity of Global Terpenoid BVOC Emissions to Environmental Stresses

Figures 4.13 a, c and e show 5-year mean values of global emissions of IP, MT and ST from 1200 to 1990 calculated by MEGAN under the controlled simulation scenario (See table 3.5), the 1000-1800 and 1950-1990 mean global emission of the controlled simulations are summarized in the first 5 rows of table 4.1. The results indicate how SAT, DV, SW content and $CO_2$ affect separately the global emissions of terpenoid BVOC. Neglecting all effects (Simulation 1: Black line 4.13 a, c and e.), the estimated millennial averaged global emissions are 505 Tg $yr^{-1}$ of IP, 76 Tg $yr^{-1}$ of MT and 12 Tg $yr^{-1}$ of ST. These results for IP and MT fall between the limits of total global annual emissions in the existing literature summarized in table 1.1.

Compared to simulation 1, an increment of all terpenoid BVOC emissions due to the effect of a SAT daily cycle is observed. IP, MT and ST global averaged emissions increase approximately 25%, 8% and 22% respectively if only a daily Surface Air Temperature (SAT) cycle is considered

**Table 4.1:** Yearly averages of the global IP, MT and ST emissions under the simulated scenarios for two periods: 1000-1800 and 1950-1990 (See table 3.5)

| Simulation ID | Mean Isoprene Global Emissions (Tg $yr^{-1}$) | | Mean Monoterpenes Global Emissions (Tg $yr^{-1}$) | | Mean Sesquiterpenes Global Emissions (Tg $yr^{-1}$) | |
|---|---|---|---|---|---|---|
| | 1000-1800 | 1950-1990 | 1000-1800 | 1950-1990 | 1000-1800 | 1950-1990 |
| 1 | 502 | 505 | 75 | 75 | 11 | 12 |
| 2 | 628 | 632 | 82 | 82 | 14 | 14 |
| 3 | 708 | 617 | 76 | 76 | 12 | 12 |
| 4 | 385 | 387 | - | - | - | - |
| 5 | 558 | 542 | - | - | - | - |
| 6 | 453 | 502 | 63 | 69 | 8 | 10 |
| 7 | 578 | 636 | 70 | 77 | 11 | 12 |
| 8 | 727 | 676 | 70 | 77 | 11 | 13 |
| 9 | 534 | 512 | - | - | - | - |
| 10 | 595 | 550 | - | - | - | - |

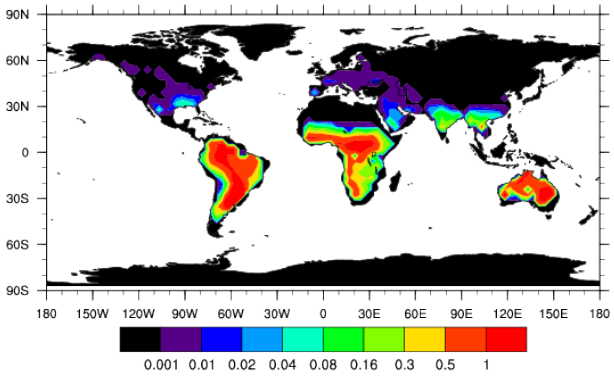


(a) Mean January ST emissions (1000-1990)

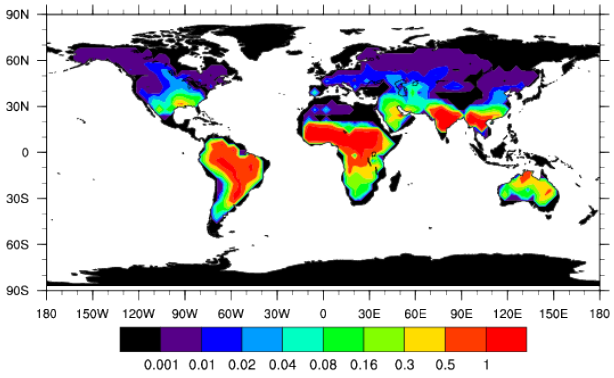


(b) Mean April ST emissions (1000-1990)

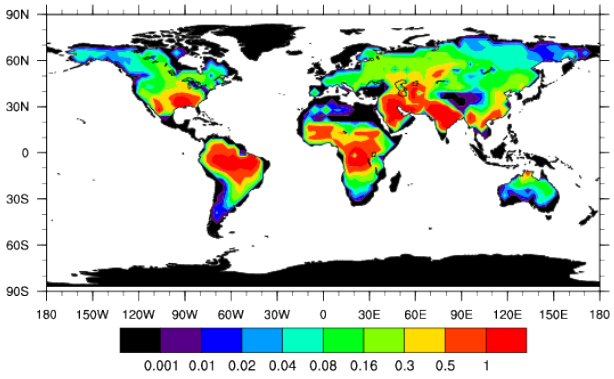


(c) Mean July ST emissions (1000-1990)

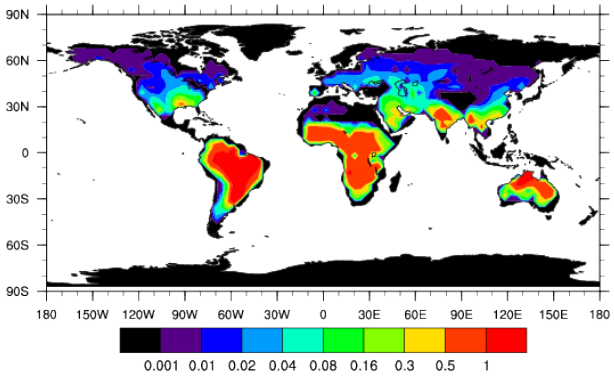


(d) Mean October ST emissions (1000-1990)

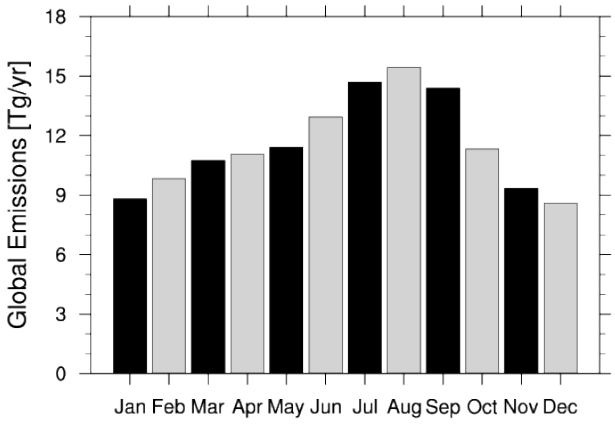


(e) Seasonality of ST emission (1000-1990)

**Figure 4.11:** Mean ST millennial emissions in (a) January, (b) April, (c) July, (d) October and (e) total monthly emissions for simulation # 8.

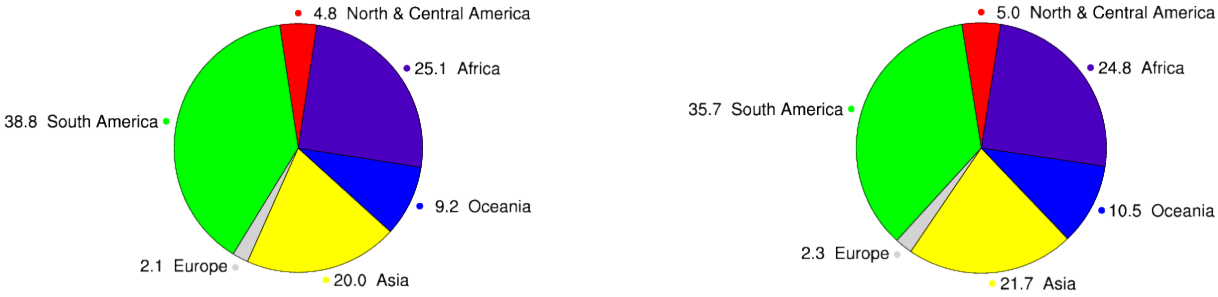


(a) Regional ST 1000-1800 emission distribution

(b) Regional ST 1950-1990 emission distribution

**Figure 4.12:** (a) Regional ST 1000-1800 emission distribution and (b) regional ST 1950-1990 emission distribution for simulation # 8.

(Simulation 2: Red line 4.13 a, c and e). The increment in all terpenoid emissions due to the single effect of SAT cycle indicate that a non-linear response of IP, MT and ST emissions to the daily variability of SAT instead of daily mean would describe reality more accurately when performing global estimates. An increment of 25% in IP global emissions agrees with results obtained by Wang et al. (1998), they estimated values of +20%.

The implementation of a dynamic vegetation (DV) module into MEGAN model shows different results for the sensitivity tests depending on the compound family (Simulation 3: Green line 4.13 a, c and e). IP emissions decrease throughout the millennium because high IP emitting vegetation is either removed or replaced by low IP emitting species in many regions of the world. Average preindustrial (1200-1800) IP emissions (697 Tg $yr^{-1}$) are 13% higher than averaged emissions during 1950-1990 (617 Tg $yr^{-1}$) when only DV is considered. MT and ST emissions are not affected by DV during the whole simulation time, showing less than 1% change from preindustrial to present day conditions because the emission factors of those compounds are in the same order of magnitude for natural and non-natural vegetation.

The effect on IP emissions of water available in the soil for plant uptake and the soil type inherent water conductivity (Wilting point) is parametrized in the model. It predicts a significant inhibition on a global scale of the order of 23% that indicates the importance of drought for the biological activity of plants (Simulation 4: Blue line 4.13 a). Average preindustrial IP emissions are 3% higher than averaged emissions during 1950-1990 due to the effect of $CO_2$ atmospheric concentration (Simulation 5: Orange line 4.13 a). The $CO_2$ effect predicted in this work agrees with previous laboratory and in-situ studies that consistently show the decreasing effect of IP emissions as atmospheric $CO_2$ increase (Peñuelas et al., 2010).

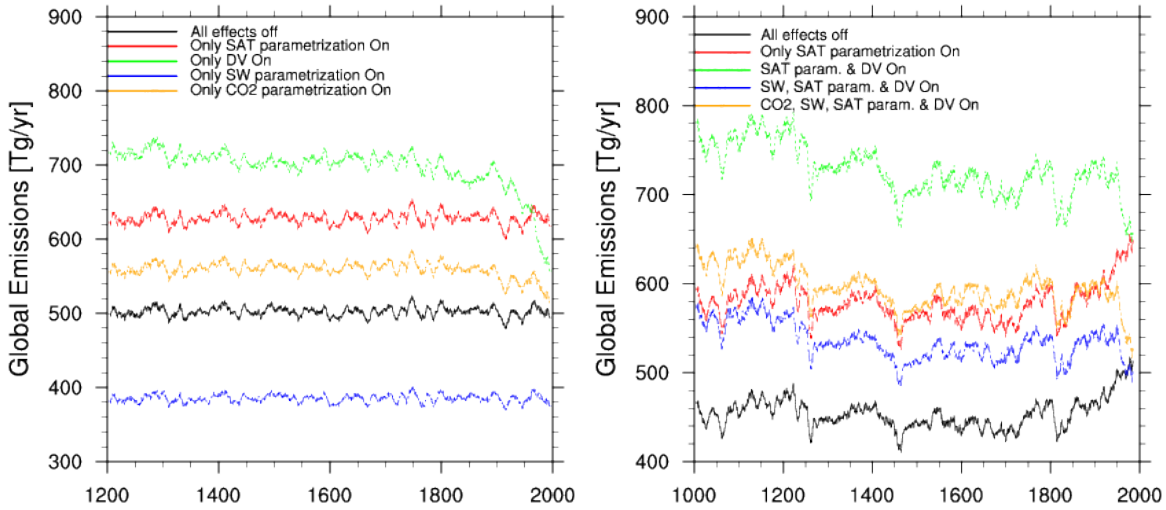


(a) Isoprene-runs 1-5




(b) Isoprene-runs 6-10

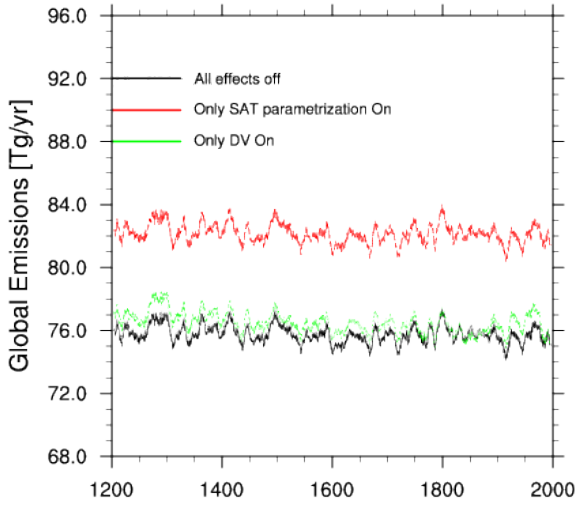


(c) Monoterpenes-runs 1-3

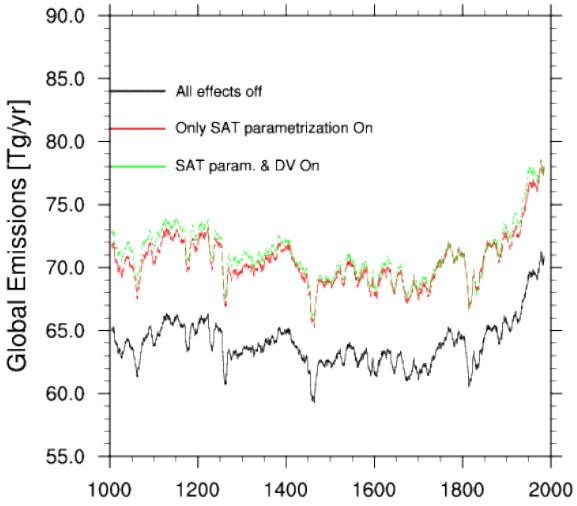


(d) Monoterpenes-runs 6-8

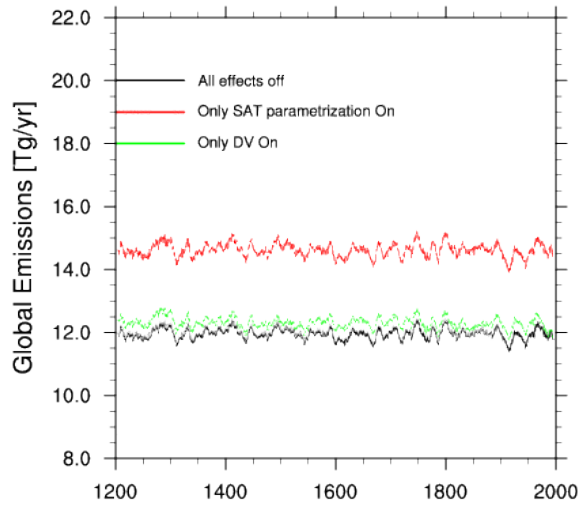


(e) Sesquiterpenes-runs 1-3

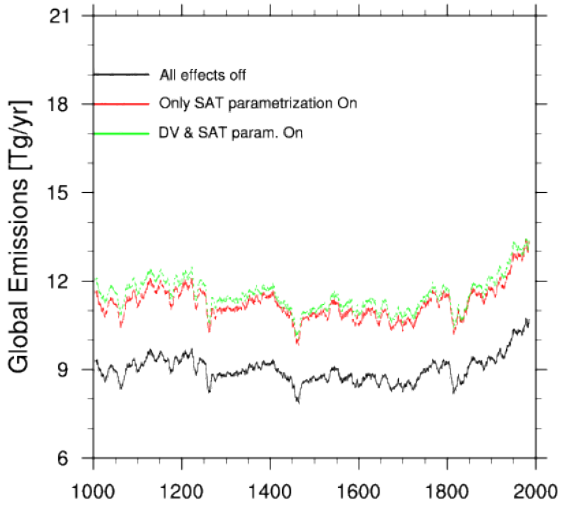


(f) Sesquiterpenes-runs 6-8

**Figure 4.13:** Millennial 5-year averaged values of the mean annual global emissions for (a) IP in the simulations 1-5, (c) MT in the simulations 1-3, (e) ST in the simulations 1-3, (b) IP in the simulations 6-10, (d) MT in the simulations 6-8 and (f) ST in the simulations 6-8.

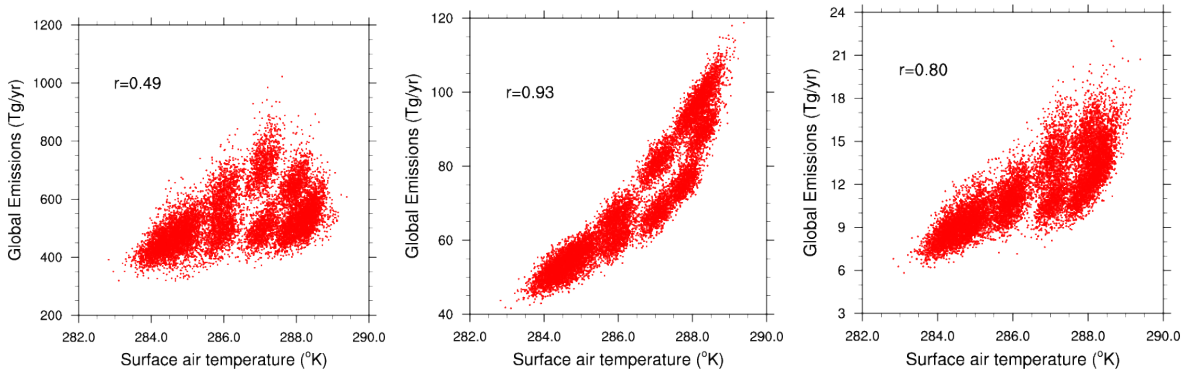


(a) Isoprene (b) Monoterpenes (c) Sesquiterpenes

**Figure 4.14:** (a) Global IP monthly emissions as a function of SAT. (a) Global MT monthly emissions as a function of SAT. (c) Global ST monthly emissions as a function of SAT.

Figures 4.13 b, d and f show 5-year mean values of global emissions of IP, MT and ST from 1000 to 1990 calculated by MEGAN under the full forcing scenario, the summary of 1000-1800 and 1950-1990 mean global emission of the full forcing simulations (See table 3.5) are summarized in the last 5 rows of 4.1. If a fixed present day vegetation (1990) is used and SW and $CO_2$ effects are neglected having only climate variability (Simulation 6: Black line in figures 4.13 b, d and f), IP, MT and ST global mean emissions follow very closely the global mean SAT. The increment from preindustrial to recent times is 11.5%, 9.1% and 16.6% for IP, MT and ST respectively.

Including a SAT daily cycle parameterization (Simulation 7: Red line in figures 4.13 b, d and f) shifts the black line in all cases upwards resembling the results of the controlled simulation discussed at the beginning of section 4.2. A comparison between the red and green line in figures 4.13 b, d and f (Simulation 8) indicates how land-use change affects global IP, MT and ST emissions. Land-use affects exclusively IP emissions, but has no effect on MT and ST emissions in both, full forcing and controlled simulations because anthropogenic vegetation with similar emitting capacity as natural vegetation replaces natural vegetation. The best estimates performed in this study by including all the known effects result in an increment from preindustrial (1000-1800) to present day (1950-1990) of 9.8% and 15.1% on MT and ST global emissions respectively (Simulation 8: Blue line in figure 4.13 c and f) and a reduction of 7.3% of IP global emissions (Simulation 10: Orange line in figure 4.13 b). Furthermore, local and regional emission variability of IP, MT and ST in the last millennium has been affected by humans and can be significantly larger than the overall variability on certain locations.

To investigate further the role of the SAT as a key regulating parameter controlling the global emissions of IP, MT and ST, scatter plots of global monthly averaged emissions of IP in simulation

# 9 and MT and ST in simulation # 8 as a function of global averages of SAT with their respective correlation coefficients are shown in panels a, b and c in figure 4.14 respectively. A clear dependence of MT emissions (r=0.93) and ST emissions (r=0.80) on SAT is observed and confirms the relevance of SAT as the major driver of changes in the emissions of those compounds. On the contrary, IP emissions have a lower correlation (r=0.49), meaning that not only SAT change has governed the emissions activity of the most abundant BVOC in the atmosphere but also land-use change has played an important role in shaping the evolution of IP in the past. Note that simulation # 9 of IP emissions is deliberately chosen so any carbon dioxide effect could be excluded in the scatter plots.

The current scientific understanding behind SOA processes indicates that high IP concentrations suppress new particle formation in vegetated regions by reacting with the OH radical (Kiendler-Scharr et al. 2009). Furthermore, the tropospheric concentrations ratio of IP and MT appears to be a key parameter regulating SOA processes (Kiendler-Scharr et al. 2009). The spatial change of the emission ratio IP/MT predicted in this study for the two periods (1000-1800 and 1950-1990) is shown in figure 4.15. An important reduction of IP emissions as compared with MT can be observed in regions where large land-use change took place such as the USA, central Eurasia and northern Australia. This reduction of IP/MT after industrialization could have led to higher particle number concentrations via new particle formation with potential impacts on regional and global climate. As discussed in the chapter one, an increment of aerosol number concentrations over vast continental regions cools down the atmosphere by directly and indirectly interacting with incoming and outgoing radiation. It is left as a following task to quantify the global terpenoid BVOC effect on the climate via organic aerosol processes.

## 4.3 Comparison to other studies

Tanaka et al.(2012) evaluate the effects that the surface air temperature, solar radiation and cropland expansion has on the emissions of isoprene (IP) and monoterpenes (MT) between 1854 and 2000 following the same emission algorithm used in this thesis. Their results show very small changes in the emissions. IP global emissions change from 650 to 640 Tg $yr^{-1}$ (-2%) and MT global emissions increase from 78 to 80 Tg $yr^{-1}$ (3%) between 1854 and 2000. In this thesis the same effects are studied on a longer temporal scale, but also the effects on IP, MT and sesquiterpenes (ST) emissions of the daily temperature cycle instead of daily averages and the effects on IP emissions from changing $CO_2$ atmospheric concentrations and soil water content. Additionally, this study considers the effect of pasture expansion as part of the land-use change scheme. The addition of these features results in a reduction of IP emissions from 600 to 520 Tg $yr^{-1}$ (-13%) and

an increment of MT emissions from 72 to 78 Tg $yr^{-1}$ (+ 8%) between 1850 and 1990, respectively.

Pacifico et al. (2012) estimates the effect on global IP emissions of changing vegetation, rising SAT and the inhibition of carbon dioxide increasing concentrations using a different IP emission scheme based in the leaf cellular synthesis of IP controlled by temperature, solar radiation, precipitation, soil water moisture, carbon dioxide and nitrogen content of the plant. These combined

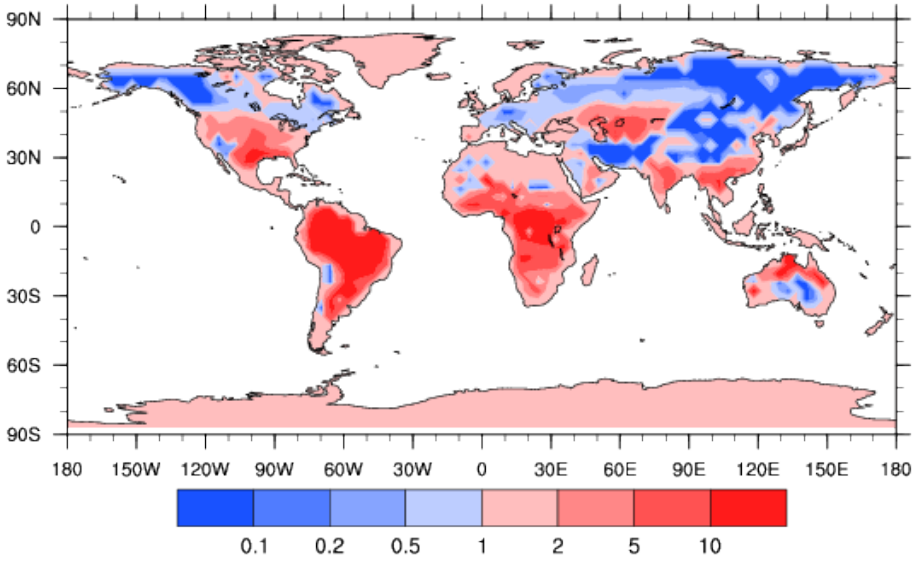


(a) Mean 1000-1800 IP/MT emissions ratio

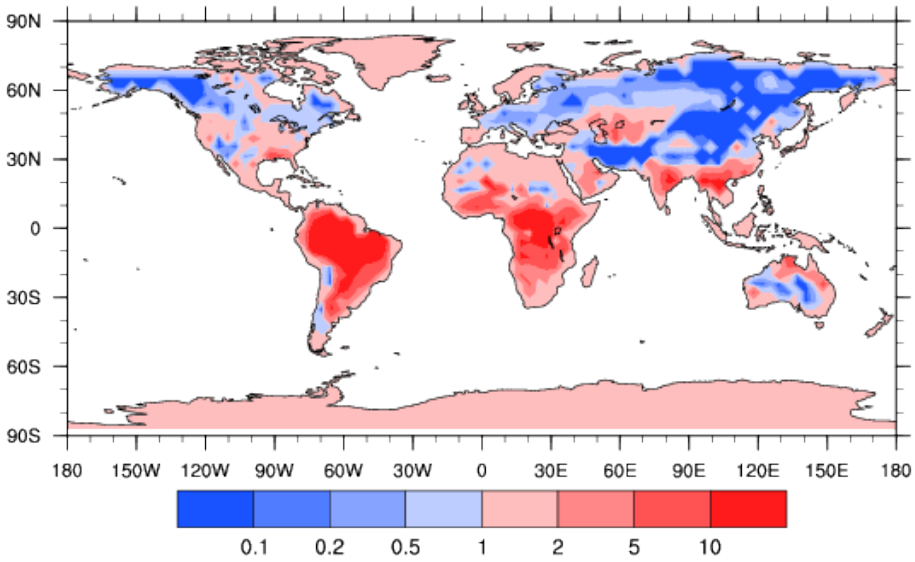


(b) Mean 1950-1990 IP/MT emissions ratio.

**Figure 4.15:** a. Mean preindustrial (1000-1800) IP/MT emissions ratio. b. Mean present day (1950-1990) IP/MT emissions ratio.

effects result in a change in the IP global emissions from 656 Tg $yr^{-1}$ to 521 Tg $yr^{-1}$ (-20%) between 1860-1869 and 2000-2009. Their results show a general good agreement with the results presented in this thesis. Carbon dioxide and land-use change have a decreasing effect on IP emissions which offsets the temperature effect. In addition, the magnitude of the emissions in pre-industrial times and present day are similar in both studies.

# 5

# Conclusions

Estimated global IP emission variation over the last millennium is dominated by the human influence on vegetation through the expansion of crops and pastures in non-vegetated regions or by replacing existing vegetation, and the rising concentrations of carbon dioxide. The rising surface air temperature had an enhancing effect of IP emissions after the industrialization that has counteracted the effect of land-use change and carbon dioxide, but its magnitude is lower.

IP emissions changed from 596 Tg $yr^{-1}$ during 1000-1800 to 550 Tg $yr^{-1}$ during 1950-1990 (-7.3%). Contrasting with IP results, MT and ST mean global emissions were much less affected by the land-use change, making the surface air temperature change the driver of increasing emissions. Total global MT increased from 70.6 to 77.6 Tg $yr^{-1}$ (+9.8%), while sesquiterpenes varied from 11.4 to 13.2 Tg $yr^{-1}$ (+15.1%) from the preindustrial period to present day. The implementation of a daily SAT cycle routine to simulate more realistic meteorological conditions over land has proven to be an important factor when estimating isoprenoid BVOC emissions. The results of IP and MT emissions are also similar with results from existing studies.

Roughly, tropical, sub-tropical and mid latitudes IP emissions are 1 order of magnitude larger than MT emissions and 2 orders of magnitude larger than ST emissions. Over boreal regions, IP and MT emissions are on the same order of magnitude and 10 times larger than ST emissions. The mean global present day IP and MT emissions estimated in this study are within the limits of previous estimates (table 1.1). The simulations capture how the human direct and indirect impact on vegetation, drought, rising temperatures and $CO_2$ concentrations affect emissions on a global scale. Regional variation in locations where vegetation has been substantially affected by humans had significant changes in emissions of IP, MT and ST. This work shows that globally, IP, MT and ST have changed over millennial timescales, with higher regional changes, indicating the importance of developing more complete and robust methods to estimate the climate and

health effects of changing BVOC on smaller spatial scales. The climate forcing induced by the millennial variability in the IP, MT and ST emissions depend on one hand on how effectively these changes affect the cloud condensation nuclei or ice nuclei concentrations via SOA, and on the other hand on how the chemistry of the atmosphere is modified. To take a step further is necessary to couple emissions to earth system models that estimate the SOA yield from IP, MT and ST and its subsequent effect on clouds and radiation, and forcing air chemistry simulations with changing emissions to estimate the chemical evolution of terpenoid BVOC and its many oxidation products in the atmosphere.

Terpenoid BVOC emissions are sensitive to meteorological conditions and land-use change, but are more sensitive to the empirical standard emission factors. An important limitation is introduced by calculating plant emissions of the different BVOC by simplifying it in a way that running the model is feasible. Averaged emission factors were used for very wide plant families in order to run global, millennial simulations. The inherent uncertainty has to be taken into account and the results are indicators of the IP, MT and ST response to external stresses and land-use change more than exact estimates of the total amounts emitted into the atmosphere. A validation of the model with measurements and a comparison of global estimates with analogous models is left for future work. Another potential source of uncertainty is the upscaling of the model to run on a coarser resolution than its original version. Notwithstanding the model limitations, this thesis presents a complementary study to the work in the existing literature by giving new insight on the topic by making use of state-of-the-art computational tools.

# Bibliography


[1] J. M. ADAMS; J. V. H. CONSTABLE; A. B. GUENTHER; P. ZIMMERMAN. **An estimate of natural volatile organic compound emissions from vegetation since the last glacial maximum**. *Chemosphere - Global Change Science 3 (2001)*, **2**:73–91, 2001. 60

[2] J. AHN; E. J. BROOK; L. MITCHELL; J. ROSEN; J. R. MCCONNELL; K. TAYLOR; D. ETHERIDGE; M. RUBINO. **Atmospheric CO2 over the last 1000 years: A high-resolution record from the West Antarctic Ice Sheet (WAIS) Divide ice core**. *Global Biogeochemical Cycles*, **26**:GB2027, 2012. 60

[3] B.A. ALBRECHT. **Aerosols; cloud microphysics; and fractional cloudiness**. *Science*, **245**:1227–1230, 1989. 60

[4] M. O. ANDREAE; D. ROSENFELD; P. ARTAXO; A. A. COSTA; G. P. FRANK; K. M. LONGO; M. A. F. SILVA-DIAS. **Smoking rain clouds over the Amazon**. *Science*, **303**:1337–1342, 2004. 60

[5] C. ANDRONACHE; L. J. DONNER; C. J. SEMAN; V. RAMASWAMY; R. S. HEMLER. **Atmospheric sulfur and deep convective clouds in tropical Pacific: A model study**. *J. of Geophysical Research*, **104**:4005–4024, 1999. 60

[6] A. ARNETH; R. K. MONSON; G. SCHURGERS; U. NIINEMETS; P. I. PALMER. **Why are estimates of global terrestrial isoprene emissions so similar (and why is this not so for monoterpenes)?** *Atmospheric Chemistry and Physics*, **8**:4605–4620, 2008. 60

[7] K. ASHWORTH; O. WILD; C. N. HEWITT. **Sensitivity of isoprene emissions estimated using MEGAN to the time resolution of input climate data**. *Atmospheric Chemistry and Physics*, **10(3)**:1193–1201, 2010. 60

[8] A. L. BERGER. **Long-term variations of caloric insolation resulting from the earth's orbital elements**. *Quaternary Research*, **9**:139–167, 1978. 60

[9] K. S. CARSLAW; O. BOUCHER; D. V. SPRACKLEN; G. W. MANN; J. G. L. RAE; S. WOODWARD; M. KULMALA. **A review of natural aerosol interactions and feedbacks within the Earth system**. *Atmospheric Chemistry and Physics*, **6**:3181–3210, 2004. 60

[10] R. FALL; R. K. MONSON. **Isoprene emission rate and intercellular isoprene concentration as influenced by stomatal distribution and conductance**. *Plant Physiology*, **100**:987–992, 1992. 60

[11] F. FEHSENFELD; J. CALVERT; R. FALL; P. GOLDAN; A. B. GUENTHER; C. N. HEWITT; B. LAMB; S. LIU; M. TRAINER; H. WESTBERG; P. ZIMMERMAN. **Emissions of volatile organic compounds from vegetation and the implications for atmospheric chemistry**. *Global Biogeochem. Cycles*, **6**:389–430, 1992. 60

[12] J. A. FOLEY; M. H. COSTA; C. DELIRE; N. RAMANKUTTY; P. SNYDER. **Green Surprise? How terrestrial ecosystems could affect Earths climate**. *Frontiers Ecol. Environ.*, **1**:38–44, 2003. 60

[13] M.-J. GAILLARD; S. SUGITA; F. MAZIER; A.-K. TRONDMAN; A. BROSTROM; T. HICKLER; J. O. KAPLAN; E. KJELLSTROM; U. KOKFELT; P. KUNES; C. LEMMEN; P. MILLER; J. OLOFSSON; A. POSKA; M. RUNDGREN; B. SMITH; G. STRANDBERG; R. FYFE; A. B. NIELSEN; T. ALENIUS; L. BALAKAUSKAS; L. BARNEKOW; H. J. B. BIRKS; A. BJUNE; L. BJORKMAN; T. GIESECKE; K. HJELLE; L. KALNINA; M. KANGUR; W. O. VAN DER KNAAP; T. KOFF; P. LAGERAS; M. LATALOWA; M. LEYDET; J. LECHTERBECK; M. LINDBLADH; B. ODGAARD; S. PEGLAR; U. SEGERSTROM; H. VON STEDINGK; AND H. SEPPA. **Holocene land-cover reconstructions for studies on land cover-climate feedbacks**. *Climate of the Past Discussions*, **6**:307–346, 2010. 60

[14] C. GERON; R. RASMUSSEN; R. R. ARNTS; A. GUENTHER. **A review and synthesis of monoterpene speciation from forests in the United States**. *Atmospheric Environment*, **34(11)**:1761–1781, 2000. 60

[15] F.J. GONZALEZ-ROUCO; L. FERNANDEZ-DONADO; C.C. RAIBLE; D. BARRIOPEDRO ; J. LUTERBACHER; J. H. JUNGCLAUS; D. SWINGEDOUW; J. SERVONNAT; E. ZORITA; S. WAGNER; C. M. AMMANN. **Medieval Climate Anomaly to Little Ice Age transition as simulated by current climate models**. *Science*, **19(1)**:7–8, 2011. 60

[16] A. GUENTHER; C. N. HEWITT; D. ERICKSON; R. FALL; C. GERON; T. GRAEDEL; P. HARLEY; L. KLINGER; M. LERDAU; W. A. MCKAY; T. PIERCE; B. SCHOLES; R. STEINBRECHER; R. TALLAMRAJU; J. TAYLOR; P. ZIMMERMAN. **A global model of natural volatile organic compound emissions**. *J. of Geophysical Research*, **100(D5)**:8873–8892, 1995. 60

[17] A. GUENTHER; T. KARL; P. HARLEY; C. WIEDINMYER; P. I. PALMER; C. GERON. **Estimates of global terrestrial isoprene emissions using MEGAN (Model of Emissions of Gases and Aerosols from Nature)**. *Atmospheric Chemistry and Physics*, **6**:3181–3210, 2006. 60

[18] A. B. GUENTHER; X. JIANG; C. L. HEALD; T. SAKULYANONTVITTAYA; T. DUHL; L. K. EMMONS; X. WANG. **The Model of Emissions of Gases and Aerosols from Nature version 2.1 (MEGAN2.1): an extended and updated framework for modeling biogenic emissions**. *Geoscientific Model Development*, **5**:1471–1492, 2012. 60

[19] M. HALLQUIST; J. C. WENGER; U. BALTENSPERGER; Y. RUDICH; D. SIMPSON; M. CLAEYS; J. DOMMEN; N. M. DONAHUE; C. GEORGE; A. H. GOLDSTEIN; J. F. HAMILTON; H. HERRMANN; T. HOFFMANN; Y. IINUMA; M. JANG; M. E. JENKIN; J. L. JIMENEZ; A. KIENDLER-SCHARR; W. MAENHAUT; G. MCFIGGANS; TH. F. MENTEL; A. MONOD; A. S. H. PREVOT; J. H. SEINFELD; J. D. SURRATT; R. SZMIGIELSKI; AND J. WILDT. **The formation; properties and impact of secondary organic aerosol: current and emerging issues**. *Atmospheric Chemistry and Physics*, **9**:5155–5236, 2009. 60

[20] J. HANSEN; M. K. I. SATO; R. RUEDY. **Estimates of the direct and indirect radiative forcing due to tropospheric aerosols: A review**. *J. of Geophysical Research*, **102**:6831–6864, 1997. 60

[21] J. HAYWOOD; O. BOUCHER. **Estimates of the direct and indirect radiative forcing due to tropospheric aerosols: A review**. *Reviews of Geophysics*, **38 (4)**:513–543, 2000. 60

[22] C. N. HEWITT; D. RUSSELL; K. MONSON; R. FALL. **Isoprene emissions from the grass Arundo donax L. are not linked to photorespiration**. *Plant Sci*, **66**:139–144, 1990. 60

[23] S. SOLOMON; D. QIN; M. MANNING; Z. CHEN; M. MARQUIS; K. B. AVERYT; M. TIGNOR; H. L. MILLER. *IPCC; 2007: The Physical Science Basis. Contribution of Working Group I to the Fourth Assessment Report of the Intergovernmental Panel on Climate Change.* Cambridge University Press; Cambridge; UK and New York; NY, 2007. 60

[24] J. L. JIMENEZ; M. R. CANAGARATNA; N. M. DONAHUE; A. S. H. PREVOT; Q. ZHANG; J. H. KROLL; P. F. DECARLO; J. D. ALLAN; H. COE; N. L. NG; A. C. AIKEN; K. S. DOCHERTY; I. M. ULBRICH; A. P. GRIESHOP; A. L. ROBINSON; J. DUPLISSY; J. D. SMITH; K. R. WILSON; V. A. LANZ; C. HUEGLIN; Y. L. SUN; J. TIAN; A. LAAKSONEN; T. RAATIKAINEN; J. RAUTIAINEN; P. VAATTOVAARA; M. EHN; M. KULMALA; J. M. TOMLINSON; D. R. COLLINS; M. J. CUBISON; J. DUNLEA; J. A. HUFFMAN; T. B. ONASCH; M. R. ALFARRA; P. I. WILLIAMS; K. BOWER; Y. KONDO; J. SCHNEIDER; F. DREWNICK; S. BORRMANN; S. WEIMER; K. DEMERJIAN; D. SALCEDO; L. COTTRELL; R. GRIFFIN; A. TAKAMI; T. MIYOSHI; S. HATAKEYAMA; A. SHIMONO; J. Y SUN; Y. M. ZHANG; K. DZEPINA; J. R. KIMMEL; D. SUEPER; J. T. JAYNE; S. C. HERNDON; A. M. TRIMBORN; L. R. WILLIAMS; E. C. WOOD; A. M. MIDDLEBROOK; C. E. KOLB; U. BALTENSPERGER; D. R. WORSNOP. **Evolution of Organic Aerosols in the Atmosphere**. *Science*, **362**:1525–1530, 2009. 60

[25] J. H. JUNGCLAUS; S. J. LORENZ; C. TIMMRECK; C. H. REICK; V. BROVKIN; K. SIX; J. SEGSCHNEIDER; M. A. GIORGETTA; T. J. CROWLEY; J. PONGRATZ; N. A. KRIVOVA; L. E. VIEIRA; S. K. SOLANKI; D. KLOCKE; M. BOTZET; M. ESCH; V. GAYLER; H. HAAK; T. J. RADDATZ; E. ROECKNER; R. SCHNUR; H. WIDMANN; M. CLAUSSEN; B. STEVENS; J. MAROTZKE. **Climate and carbon-cycle variability over the last millennium**. *Climate of the Past*, **6**:723–737, 2010. 60

[26] J. O. KAPLAN; G. FOLBERTH; D. A. HAUGLUSTAINE. **Role of methane and biogenic volatile organic compound sources in late glacial and Holocene fluctuations of atmospheric methane concentrations**. *Global Biogeochemical cycles*, **20**:GB2016, 2006. 60

[27] J. O. KAPLAN; K. M. KRUMHARDT; E. C. ELLIS; W. F. RUDDIMAN; C. LEMMEN; K. KLEIN-GOLDEWIJK. **Holocene carbon emissions as a result of anthropogenic land cover change**. *The Holocene*, **21(5)**:775–791, 2010. 60

[28] T. KARL; M. POTOSNAK; A. GUENTHER; D. CLARK; J. WALKER; J. D. HERRICK; C. GERON. **Exchange processes of volatile organic compounds above a tropical rain forest:: Implications for modeling tropospheric chemistry above dense vegetation**. *Atmospheric Chemistry and Physics*, **6**:3181–3210, 2004. 60

[29] V.-M. KERMINEN; M. KULMALA. **Analytical formulae connecting the real and the apparent nucleation rate and the nuclei num. concentration for atmospheric nucleation events**. *J. of Aerosol Science*, **33**:609–622, 2002. 60

[30] V.-M. KERMINEN; M. PARAMONOV; T. ANTTILA; I. RIIPINEN; C. FOUNTOUKIS; H. KORHONEN; E. ASMI; L. LAAKSO; H. LIHAVAINEN; E. SWIETLICKI; B. SVENNINGSSON; A. ASMI; S. N. PANDIS; M. KULMALA; T. PETAJA. **Cloud condensation nuclei production associated with atmospheric nucleation: a synthesis based on existing literature and new results**. *Atmospheric Chemistry and Physics*, **12**:12037–12059, 2012. 60

[31] J. KESSELMEIER; M. STAUDT. **Biogenic Volatile Organic Compounds (VOC): An Overview on Emission; Physiology and Ecology**. *J. of Atmospheric Chemistry*, **33**:23–88, 1999. 60

[32] J KESSELMEIER; U. KUHN; S. ROTTENBERGER; T. BIESENTHAL; A. WOLF; G. SCHEBESKE; M. O. ANDREAE; P. CICCIOLI; E. BRANCALEONI; M. FRATTONI; S.T. OLIVA; M. L. BOTELHO; C. M. A. SILVA; T.M. TAVARES. **Concentrations and species composition of atmospheric volatile organic compounds (VOCs) as observed during the wet and dry season in RondÃťnia (Amazonia)**. *J. of Geophysical Research*, **107 (D20)**:8053, 2002. 60

[33] A. KIENDLER-SCHARR; J. WILDT; M. DAL MASO; T. HOHAUS; E. KLEIST; T. F. MENTEL; R. TILLMANN; R. UERLINGS; U. SCHURR; A. WAHNER. **New particle formation in forests inhibited by isoprene emissions**. *Nature*, **461**:381–384, 2009. 60

[34] M. KULMALA; A. LAAKSONEN; R. J.CHARLSON; P. KORHONEN. **Clouds without supersaturation**. *Nature*, **388**:336–337, 1997. 60

[35] M. KULMALA; T. SUNI; K. E. J. LEHTINEN; M. DAL MASO; M. BOY; A. REISSELL; U. RANNIK; P. AALTO; P. KERONEN; H. HAKOLA; J. BACK; T. HOFFMANN; T. VESALA; AND P. HARI. **A new feedback mechanism linking forests; aerosols; and climate**. *Atmospheric Chemistry and Physics*, **4**:557–562, 2004. 60

[36] M. KULMALA; I. RIIPINEN; M. SIPILA; H. E. MANNINEN; T. PETAJA; H. JUNNINEN; M. DAL MASO; G. MORDAS; A. MIRME; M. VANA; A. HIRSIKKO; L. LAAKSO; R. M. HARRISON; I. HANSON; C. LEUNG; K. E. J. LEHTINEN; V.-M. KERMINEN. **Toward Direct Measurement of Atmospheric Nucleation**. *Science*, **318**:89–92, 2007. 60

[37] M. KULMALA AND V.-M. KERMINEN. **On the formation and growth of atmospheric nanoparticles**. *Atmospheric Research*, **90**:132–150, 2008. 60

[38] J. LAOTHAWORNKITKUL; J. E. TAYLOR; N. D. PAUL; C. N. HEWITT. **Biogenic volatile organic compounds in the Earth system**. *New Phytologist*, **183**:27–51, 2009. 60

[39] U. LOHMANN; J. FEICHTER. **Global indirect aerosol effects: a review**. *Atmospheric Chemistry and Physics*, **5**:715–737, 2005. 60

[40] R. MAKKONEN; A. ASMI; V.-M. KERMINEN; M. BOY; A. ARNETH; P. HARI; M. KULMALA. **Air pollution control and decreasing new particle formation lead to strong climate warming**. *Atmospheric Chemistry and Physics*, **12**:1515–1524, 2012. 60

[41] C. MACFARLING MEURE; D. ETHERIDGE; C. TRUDINGER; P. STEELE; R. LANGENFELDS; T. VAN OMMEN; A. SMITH; J. ELKINS. **Law Dome CO2; CH4 and N2O ice core records extended to 2000 years BP**. *Geophysical Research Letters*, **33**:L14810, 2006. 60

[42] J. R. ODUM; T. HOFFMANN ; F. BOWMAN ; D. COLLINS ; R. C. FLAGAN; J. H. SEINFELD. **Gas/Particle Partitioning and Secondary Organic Aerosol Yields**. *Environmental Science and Technology*, **30**:2580–2585, 1996. 60

[43] P. I. PALMER; D. J. JACOB; A. M. FIORE; R. V. MARTIN; K. CHANCE; T. P. KUROSU. **Mapping isoprene emissions over North America using formaldehyde column observations from space**. *J. of Geophysical Research*, **108(D6)**:4180, 2003. 60

[44] W.J. PARTON; J. A. LOGAN. **A model for diurnal variation in soil and air temperature**. *Agricultural Meteorology*, **23**:205–216, 1981. 60

[45] J. PENUELAS; T. RUTISHAUSER; I. FILELLA. **Phenology Feedbacks on Climate Change**. *Science*, **324**:887–888, 2009. 60

[46] J. PENUELAS; M. STAUDT. **BVOCs and global change**. *Trends in Plant Science*, **15 (3)**:133–144, 2010. 60

[47] J. PONGRATZ; C. REICK; T. RADDATZ; M. CLAUSSEN. **A reconstruction of global agricultural areas and land cover for the last millennium**. *Global Biogeochemical Cycles*, **22**:16, 2008. 60

[48] J. PONGRATZ; T. RADDATZ; C. H. REICK; M. ESCH; M. CLAUSSEN. **Radiative forcing from anthropogenic land cover change since A.D. 800**. *Geophysical Research Letters*, **36**:02709, 2009. 60

[49] J. PONGRATZ; C. H. REICK; T. RADDATZ; M. CLAUSSEN. **Biogeophysical versus biogeochemical climate response to historical anthropogenic land cover change**. *J. of Geophysical Research*, **37**:8702, 2010. 60

[50] F. RAES; R. VAN DINGENEN; E. VIGNATI; J. WILSON; J. PUTAUD; J. H. SEINFELD; P. ADAMS. **Formation and cycling of aerosols in the global troposphere**. *Atmospheric Environment*, **34**:4215–4240, 2000. 60

[51] N. RAMANKUTTY; J. A. FOLEY. **Estimating historical changes in global land cover: Croplands from 1700 to 1992**. *Global Biogeochemical Cycles*, **13(4)**:997–1027, 1999. 60

[52] I. RIIPINEN; J. R. PIERCE; T. YLI-JUUTI; T. NIEMINEN; S. HAKKINEN; M. EHN; H. JUNNINEN; K. LEHTIPALO; T. PETAJA; J. SLOWIK; R. CHANG; N. C. SHANTZ; J. ABBATT; W. R. LEAITCH; V.-M. KERMINEN; D. R. WORSNOP; S. N. PANDIS; N. M. DONAHUE; AND M. KULMALA. **Organic condensation: a vital link connecting aerosol formation to cloud condensation nuclei (CCN) concentrations**. *Atmospheric Chemistry and Physics*, **11**:3865–3878, 2011. 60

[53] H.J.I. RINNE; A.B. GUENTHER; J.P. GREENBERG; P.C. HARLEY. **Isoprene and monoterpene fluxes measured above Amazonian rainforest and their dependence on light and temperature**. *Atmospheric Environment*, **36**:2421–2426, 2002. 60

[54] R. R. ROGERS; M. K. YAU. *A Short Course in Cloud Physics*. International S. in Natural Philosophy), 1989. 60

[55] T. N. ROSENSTIEL; M. J. POTOSNAK ; K. L. GRIFFIN; R. FALL; R. K. MONSON. **Increased CO2 uncouples growth from isoprene emission in an agriforest ecosystem**. *Nature*, **421**:256–259, 2003. 60

[56] T. SAKULYANONTVITTAYA; T. DUHL; C. WIEDINMYER; D. HELMIG; S. MATSUNAGA; M. POTOSNAK; J. MILFORD; A. GUENTHER. **Monoterpene and Sesquiterpene Emission Estimates for the United States**. *Environmental Science Technology*, **42**:1623–1629, 2008. 60

[57] J. H. SEINFELD; S. N. PANDIS. *Atmospheric Chemistry and Physics: From Air Pollution to Climate Change*. Wiley; New York, 2006. 60

[58] T. D. SHARKEY; A. E. WIBERLEY; A. R. DONOHUE. **Isoprene Emission from Plants**. *Plant Biology*, **52**:407–436, 2001. 60

[59] K. TANAKA; H.-J. KIM; K. SAITO; H. G. TAKAHASHI; M. WATANABE; T. YOKOHATA; M. KIMOTO; K. TAKATA; T. YASUNARI. **How have both cultivation and warming influenced annual global isoprene and monoterpene emissions since the preindustrial era?** *Atmospheric Chemistry and Physics Discussions*, **12**:16515–16555, 2012. 60

[60] D. T. TINGEY; M. MANNING; L. C. GROTHAUS; W. F. BURNS. **Influence of light and temperature on monoterpene emission rates from slash pine**. *Plant Physiology*, **65**:797–801, 1980. 60

[61] Y. WANG; D. JACOB. **Anthropogenic forcing on tropospheric ozone and OH since preindustrial times**. *J. of Geophysical Research*, **103(31)**:123–135, 1998. 60

[62] S. TWOMEY. **The nuclei of natural cloud formation part II: The supersaturation in natural clouds and the variation of cloud droplet concentration**. *Pure and Applied Geophysics*, **43**:243–249, 1957. 60

[63] P. J. VALDES; DAVID J. BEERLING; COLIN E. JOHNSON. **The ice age methane budget**. *Geophysical Research Letters*, **32**:L02704, 2005. 60

[64] H. VEHKMAKI; I. RIIPINEN. **Thermodynamics and kinetics of atmospheric aerosol particle formation and growth**. *Chemical Society Review*, -:–, 2012. 60

[65] A. WEISS; J. M. NORMAN. **Partitioning solar radiation into direct and diffuse; visible and near-infrared components**. *Agricultural and Forest Meteorology*, **34**:205–213, 1985. 60

[66] J. Z. YU; D. R. COCKER; R. J. GRIFFIN; R. C. FLAGAN; J. H. SEINFELD. **Gas-Phase Ozone Oxidation of Monoterpenes Gaseous and Particulate Products**. *J. of Atmospheric Chemistry*, **34**:207–258, 1999. 60